nature nanotechnology

Article

https://doi.org/10.1038/s41565-023-01560-7

Associating growth factor secretions and transcriptomes of single cells in nanovials using SEC-seq

Received: 3 April 2023

Accepted: 31 October 2023

Published online: 11 December 2023

Check for updates

Shreya Udani[1,9], Justin Langerman[2,9], Doyeon Koo[1], Sevana Baghdasarian[3], Brian Cheng[1], Simran Kang[1], Citradewi Soemardy[1], Joseph de Rutte[4], Kathrin Plath[2,5,6] ✉ & Dino Di Carlo[1,4,5,7,8] ✉

Cells secrete numerous bioactive molecules that are essential for the function of healthy organisms. However, scalable methods are needed to link individual cell secretions to their transcriptional state over time. Here, by developing and using secretion-encoded single-cell sequencing (SEC-seq), which exploits hydrogel particles with subnanolitre cavities (nanovials) to capture individual cells and their secretions, we simultaneously measured the secretion of vascular endothelial growth factor A (VEGF-A) and the transcriptome for thousands of individual mesenchymal stromal cells. Our data indicate that VEGF-A secretion is heterogeneous across the cell population and is poorly correlated with the *VEGFA* transcript level. The highest VEGF-A secretion occurs in a subpopulation of mesenchymal stromal cells characterized by a unique gene expression signature comprising a surface marker, interleukin-13 receptor subunit alpha 2 (IL13RA2), which allowed the enrichment of this subpopulation. SEC-seq enables the identification of gene signatures linked to specific secretory states, facilitating mechanistic studies, the isolation of secretory subpopulations and the development of means to modulate cellular secretion.

Over 3,000 proteins are predicted to be secreted from human cells[1], and secretions such as cytokines and growth factors affect many critical functions[2]. Mesenchymal stromal cells (MSCs) are evaluated as therapeutics because they secrete bioactive factors, including growth factors, cytokines and extracellular vesicles, that promote immunomodulation and regeneration[3,4]. Yet, successful translation of MSCs and other cell therapies have been hindered by clinical inconsistency attributed to functional differences in cell source and heterogeneity. Reaching the therapeutic potential of cell therapies necessitates an understanding of the subpopulations that secrete specific proteins, and ideally quantification of protein secretion at the single-cell level. A method that links transcription and secretions of individual cells at scale would be highly valuable, both for identifying new regulatory mechanisms of protein secretion and for developing the next generation of cell therapies[2,5].

[1]Department of Bioengineering, University of California Los Angeles, Los Angeles, CA, USA. [2]Department of Biological Chemistry, David Geffen School of Medicine, University of California Los Angeles, Los Angeles, CA, USA. [3]Department of Chemical and Biomolecular Engineering, University of California Los Angeles, Los Angeles, CA, USA. [4]Partillion Bioscience, Los Angeles, CA, USA. [5]Jonsson Comprehensive Cancer Center, University of California Los Angeles, Los Angeles, CA, USA. [6]Eli and Edythe Broad Stem Cell Research Center, University of California Los Angeles, Los Angeles, CA, USA. [7]Department of Mechanical and Aerospace Engineering, University of California Los Angeles, Los Angeles, CA, USA. [8]California NanoSystems Institute (CNSI), University of California Los Angeles, Los Angeles, CA, USA. [9]These authors contributed equally: Shreya Udani, Justin Langerman. ✉e-mail: kplath@mednet.ucla.edu; dicarlo@ucla.edu

https://doi.org/10.1038/s41565-023-01560-7

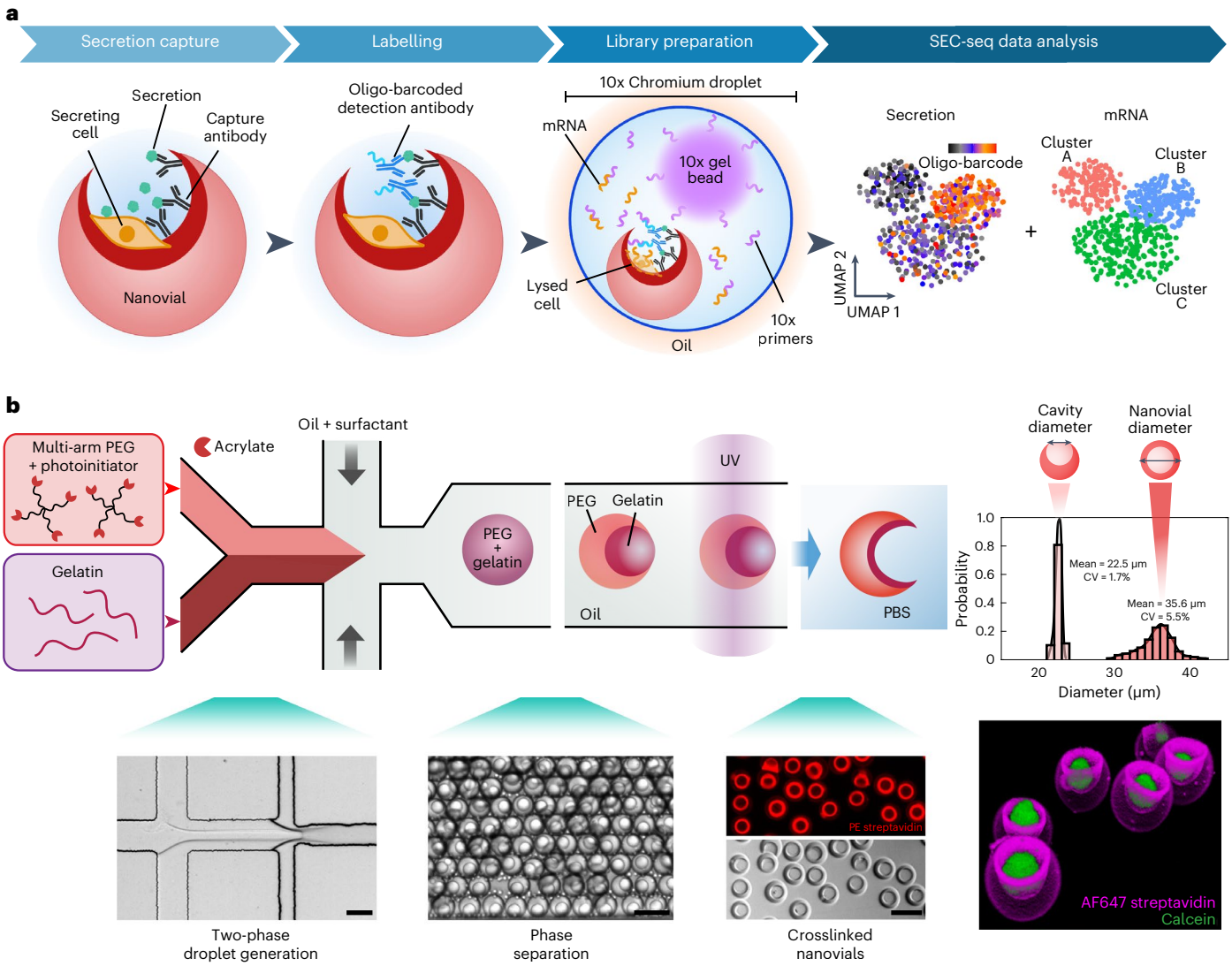

Fig. 1 | Overview of the SEC-seq workflow using nanovials. a, Cells are loaded, adhered and incubated in gelatin-coated nanovials functionalized with secretion capture antibodies. Secreted and captured proteins are labelled with oligo-barcoded detection antibodies. Nanovials loaded with single cells are then introduced into the 10x Chromium workflow for library preparation. Sequencing of the resulting libraries results in matched secretion and transcriptomics data for downstream analyses. Schematic partially created with BioRender.com. **b**, Gelatin-coated nanovials are fabricated using aqueous two-phase separation of gelatin and four-arm PEG acrylate in a flow-focusing device in which phase separation occurs followed by ultraviolet (UV) crosslinking. Post-fabrication biotinylation of nanovials via gelatin allows for visualization of cavities using phycoerythrin (PE)-labelled streptavidin. The resulting 35 µm nanovials are highly uniform with a cavity diameter coefficient of variation (CV) of 1.7% and nanovial diameter CV of 5.5%. MSCs loaded in nanovials settle in the centre of the cavity, as seen in the confocal microscopy image where fluorescent streptavidin-labelled nanovials are loaded with calcein-stained cells (bottom right). Scale bars, 50 µm.

Here we developed secretion-encoded single-cell sequencing (SEC-seq), which leverages microscale hydrogel particles (nanovials)[6–8] and single-cell RNA sequencing (scRNA-seq) in microfluidic droplet emulsions to determine both transcriptome and secretion information from thousands of individual cells (Fig. 1). Cells are loaded into gelatin-coated nanovials conjugated with capture antibodies for a secreted protein of interest, allowing the cells to adhere to the nanovial cavity and for secreted protein to be captured. Upon labelling secreted proteins with oligonucleotide (oligo)-barcoded detection antibodies, nanovials are enriched for single-cell loading by fluorescence-activated cell sorting (FACS) and then partitioned for single-cell library preparation followed by next-generation sequencing using established workflows[9,10].

We show the utility of SEC-seq by exploring the relationship between the secretion of vascular endothelial growth factor A (VEGF-A) and the underlying transcriptome state in MSCs. VEGF-A is an important secreted product that promotes angiogenesis and is involved in many MSC-based therapies[11–13]. Our findings based on simultaneous measurement of secretion and the transcriptome from thousands of single cells indicate that multiple regulatory pathways control VEGF-A secretion, highlighting the need for the detection of secretory subpopulations.

Results

Establishing the SEC-seq workflow

To develop SEC-seq, we ascertained that (1) VEGF-A secretion from single, viable MSCs can be detected on nanovials; (2) cell-loaded nanovials can be emulsified for scRNA-seq; and (3) transcripts and oligo-barcodes from them can be quantified (Fig. 2a).

We developed a flow cytometry-compatible, single-cell VEGF-A secretion assay using nanovials (Methods, Table 1 and Fig. 1b). Nanovial binding capacity was determined by purified VEGF-A addition to nanovials conjugated with capture antibodies and measuring VEGF-A

https://doi.org/10.1038/s41565-023-01560-7

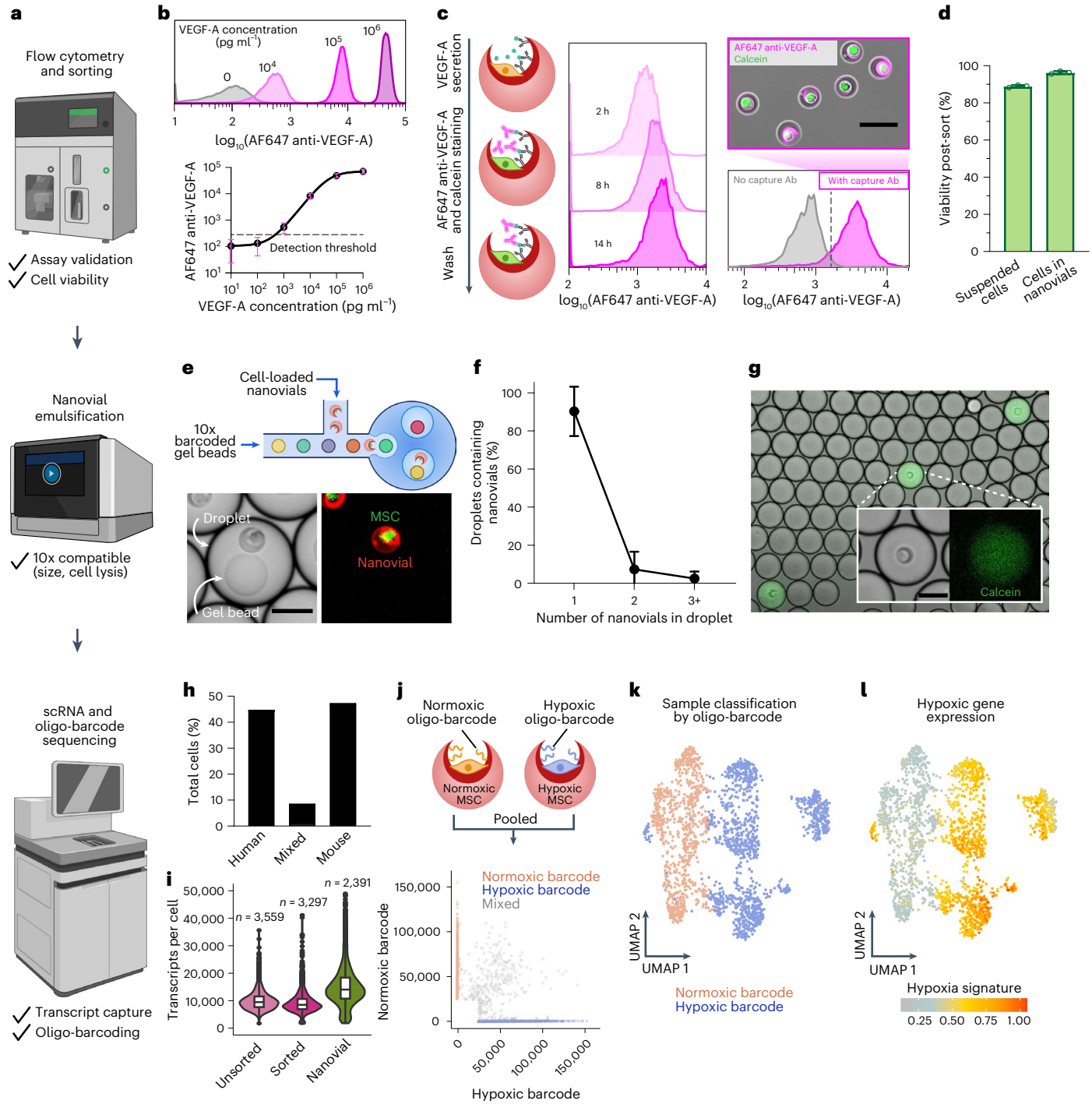

Fig. 2 | Establishing the SEC-seq workflow. a, Standard scRNA-seq equipment including Sony cell sorter, 10x Chromium and Illumina sequencers used for SEC-seq (top to bottom). **b**, Standard curve of VEGF-A on nanovials quantified by flow cytometry using recombinant VEGF-A and a sandwich immunoassay. The horizontal dashed line represents the detection threshold. **c**, Left: VEGF-A secretion assay in single MSC-loaded nanovials. Middle: flow cytometry histograms of VEGF-A secretion from single MSCs on nanovials after indicated incubation times. Bottom right: VEGF-A secretion assay on single MSC-loaded nanovials with and without VEGF-A capture antibody (Ab). The dashed line represents the detection threshold. Top right: single calcein AM-stained MSCs (green) on nanovials with secreted VEGF-A detected by a fluorescently tagged VEGF-A antibody (magenta). **d**, Cell viability following sorting of cells in suspension versus loaded in nanovials. Data presented as mean values ± s.d. for three replicates. **e**, Top: nanovial emulsification with gel beads using 10x Chromium. Bottom: nanovials with single MSCs with a training gel bead (no cell lysis) in a droplet following emulsification. **f**, Proportion of nanovial-containing droplets with the indicated number of nanovials. Data presented as mean values ± s.d. for three repeat experiments. **g**, Overlaid fluorescence and brightfield images of droplets, some containing cell-loaded nanovials, with cell lysis. **h**, Assignment of cells from the experiment where nanovials containing human or mouse cells are pooled 1:1. We retrieved 2,821 human, 2,950 mouse and 515 mixed cells. **i**, Transcripts per cell for suspended (unsorted) MSCs, suspended and sorted (sorted) MSCs, or MSCs loaded on nanovials and sorted (nanovial). Numbers above the plot indicate cells per sample. **j**, Normoxic or hypoxic MSCs loaded on nanovials labelled with different ('normoxic' and 'hypoxic') oligo-barcodes and analysed in a 1:1 ratio. The scatter plot depicts the assignment of cells based on the oligo-barcode attached to nanovials. **k**, UMAP plot of the scRNA-seq data from the experiment in **j**, where cells are labelled by their oligo-barcode assignment. We retrieved 1,249 hypoxic and 865 normoxic cells; mixed cells excluded in UMAPs. **l**, UMAP from **k** labelled by hypoxic gene expression signature. Scale bars, 50 µm for all images. Schematics in **a**, **c** and **j** created with BioRender.com.

Table 1 | Typical sensor gain settings used with SONY SH800S for nanovial sorts

Sensor	FSC	BSC	FL2	FL3	FL4
Gain	2	25%	20%	25%	32%
Stain/antibody			Calcein AM	CellTracker Orange	AF647 anti-VEGF, AF647 anti-mouse IgG

retained in nanovials by flow cytometry after incubation with fluorescently tagged detection antibody. VEGF-A was detected across a dynamic range of at least two orders of magnitude (Fig. 2b). The 35 µm gelatin-coated nanovials have a 20 µm cavity, facilitating MSC adherence via integrin binding (Extended Data Fig. 1a) with ~20% of nanovials containing single MSCs (Extended Data Fig. 1b–d), usually centred in the nanovial cavity (Fig. 1b).

VEGF-A secretion was detectable by FACS from MSCs loaded onto nanovials conjugated with the VEGF-A capture antibody, incubated and then exposed to fluorescent detection antibody; nanovial fluorescence increased with MSC-nanovial incubation time and VEGF-A could remain stably bound for over 24 hours (Fig. 2c and Extended Data Fig. 1e,f). After a 14-hour incubation, 90% of nanovials showed signal above a threshold defined by nanovials with no VEGF-A capture antibody, indicating that most MSCs are secreting VEGF-A (Fig. 2c). We observed a broad distribution of fluorescence intensity, indicating heterogeneity in VEGF-A secretion levels across individual cells (Fig. 2c), which was corroborated by the VEGF-A enzyme-linked immunosorbent spot (ELISpot) assay (Extended Data Fig. 1h). Cell-loaded nanovials had a 2.4-fold increase in mean fluorescence signal compared with empty nanovials, indicating low crosstalk between nanovials, even in the presence of low nanovial autofluorescence and non-specific binding of the detection antibody (Extended Data Fig. 1e,g). To confirm that cell viability is preserved on nanovials, which is required for high-quality scRNA-seq data[14], we sorted suspended MSCs or MSC-loaded nanovials and found both conditions had high viability post-sort (Fig. 2d). Nanovials could even protect MSCs during sorting after exposure to surfactant (Extended Data Fig. 2a). Modelling of fluid shear forces in the flow cytometer nozzle yielded a 400-fold-higher fluid dynamic shear stress acting on suspended cells versus cells loaded in nanovials (Extended Data Fig. 2b–d), suggesting that nanovials shield cells from fluidic stresses[15].

Next, we explored whether cell-loaded nanovials are compatible with emulsion generation and cell lysis for scRNA-seq using 10x Chromium, a commercially available scRNA-seq platform compatible with nanovials. The 35 µm nanovials were successfully loaded into microfluidic droplets with barcoded primer beads (Fig. 2e). Image analysis showed that the majority of droplets with nanovials contain one nanovial, and that the inclusion of multiple nanovials is similar to the expected multiplet rate reported by the manufacturer for cell loading (9.7% versus 4%; Fig. 2f). Fluorescence microscopy of emulsions formed with nanovials containing calcein-stained MSCs in the presence of cell lysis buffer showed localized release of the dye, pervading only nanovial-containing droplets, indicating successful cell lysis post emulsification (Fig. 2g). To test the generation of high-quality scRNA-seq libraries from nanovial-loaded cells, we performed a species mixing experiment where human MSCs and mouse fibroblasts were loaded separately into nanovials and combined in a 1:1 ratio before loading into 10x Chromium. After scRNA-seq, we retrieved transcripts from 6,296 cells. The species distribution reflected the initial pooling ratio with 44.8% human cells, 47% mouse cells and 8.2% mixed cells (Fig. 2h). To study how loading MSCs in nanovials affects transcript recovery, we performed scRNA-seq for suspended MSCs, suspended MSCs sorted for positive calcein signal and MSCs loaded in nanovials sorted for single cells. Although fewer cells were detected in the nanovial sample (same sequencing depth per sample), transcript and gene detection per cell was not adversely affected (Fig. 2i and Extended Data Fig. 3a). Both nanovial-loaded and suspended MSCs expressed standard MSC-specific surface markers (Extended Data Fig. 3b); yet cells on nanovials clustered separately from suspended cells (Extended Data Fig. 3c). Gene Ontology analysis showed that genes significantly upregulated in nanovial-loaded cells are related to anchorage-dependent processes such as cell division and DNA replication[16], potentially reflecting a healthier state for MSCs on nanovials (Extended Data Fig. 3d,e).

Lastly, we confirmed detection of oligo-barcodes within nanovials together with transcriptomes. Two populations of nanovials loaded with MSCs were each tagged with a distinct oligo-barcode (Fig. 2j): MSCs were cultured in either standard normoxic conditions or treated with an hypoxia-mimetic agent, known to increase the secretion of angiogenic growth factors, including VEGF-A[17,18] (Extended Data Fig. 4a). The hypoxia-driven increase of VEGF-A secretion in hypoxic conditions was confirmed with flow cytometry for MSCs in nanovials (Extended Data Fig. 4b). Eighty-five per cent of cells could be assigned to one of the two oligo-barcodes and cells defined by the two nanovial barcodes separated when plotted together in a uniform manifold approximation plot (UMAP; Fig. 2j,k). The barcode-based classification matched the expected gene expression profile, with over 90% of cells with high hypoxic gene signature expression (including *VEGFA*; Supplementary Table 1) assigned to the respective (hypoxic) barcode (Fig. 2l). In addition, 93% of cells had high levels of an oligo-barcode indicating that the majority of cells were associated with a nanovial in this process (Supplementary Fig. 3f).

VEGF-A secretion is unlinked to *VEGFA* transcripts

With the workflow validated, we used SEC-seq for simultaneously measuring secretion of VEGF-A and the global transcriptome for thousands of individual MSCs (Fig. 3a). To detect secreted VEGF-A by sequencing, we designed a VEGF-A detection antibody conjugated to a 10x Chromium-compatible oligo-barcode that specifically detects VEGF-A (Extended Data Fig. 5a–c). 10x bead capture primers add unique molecular identifiers and cell barcodes to the antibody barcode upon binding and amplification, which are counted to measure VEGF-A secretion per cell.

As in the fluorescence secretion assay, MSCs were loaded in nanovials coated with VEGF-A capture antibodies and incubated for 14 hours to collect secreted VEGF-A in normoxic and hypoxic culture conditions. Next we added oligo-barcoded anti-VEGF-A detection antibody, sorted to isolate nanovials containing single, viable MSCs, and processed for scRNA-seq. MSCs cultured in normoxic and hypoxic conditions separated in transcriptional space on UMAPs (Fig. 3b). VEGF-A secretion and *VEGFA* transcripts were more abundant in the hypoxic culture condition (Fig. 3c,d). On average, hypoxic cells secreted 1.72 times more VEGF-A than normoxic cells (Fig. 3e, middle). The VEGF-A secretion SEC-seq measurement was corroborated by the flow cytometry secretion assay using a fluorescently tagged anti-VEGF-A antibody (hypoxic 1.66 times higher; Fig. 3e, top).

Inspecting VEGF-A secretion and transcript levels, we made three key observations. First, we found that VEGF-A secretion was detected in nearly all cells (99%) and that some cells showed higher VEGF-A secretion, indicating that secretion is highly heterogeneous regardless of culture condition (Fig. 3c). Second, we detected *VEGFA* transcripts in 88% of cells and found that the heterogeneity in VEGF-A secretion was not matched by *VEGFA* transcript levels (compare Fig. 3c,d). Third, hypoxic MSCs showed 13-fold higher average *VEGFA* transcript levels and a greater range of transcript levels compared with normoxic cells (Fig. 3e, bottom), indicating that transcript levels change more than secretion levels. These results suggest a surprising uncoupling between VEGF-A secretion and *VEGFA* transcript levels and an unexpected heterogeneity in VEGF-A secretion.

We used transcriptome-based clustering to further investigate the relationship between VEGF-A secretion and *VEGFA* transcript levels (Fig. 3f). Clusters N1–N5 are predominantly normoxic cells, clusters H1–H4 are hypoxic cells and clusters M1–M3 contain cells from both

https://doi.org/10.1038/s41565-023-01560-7

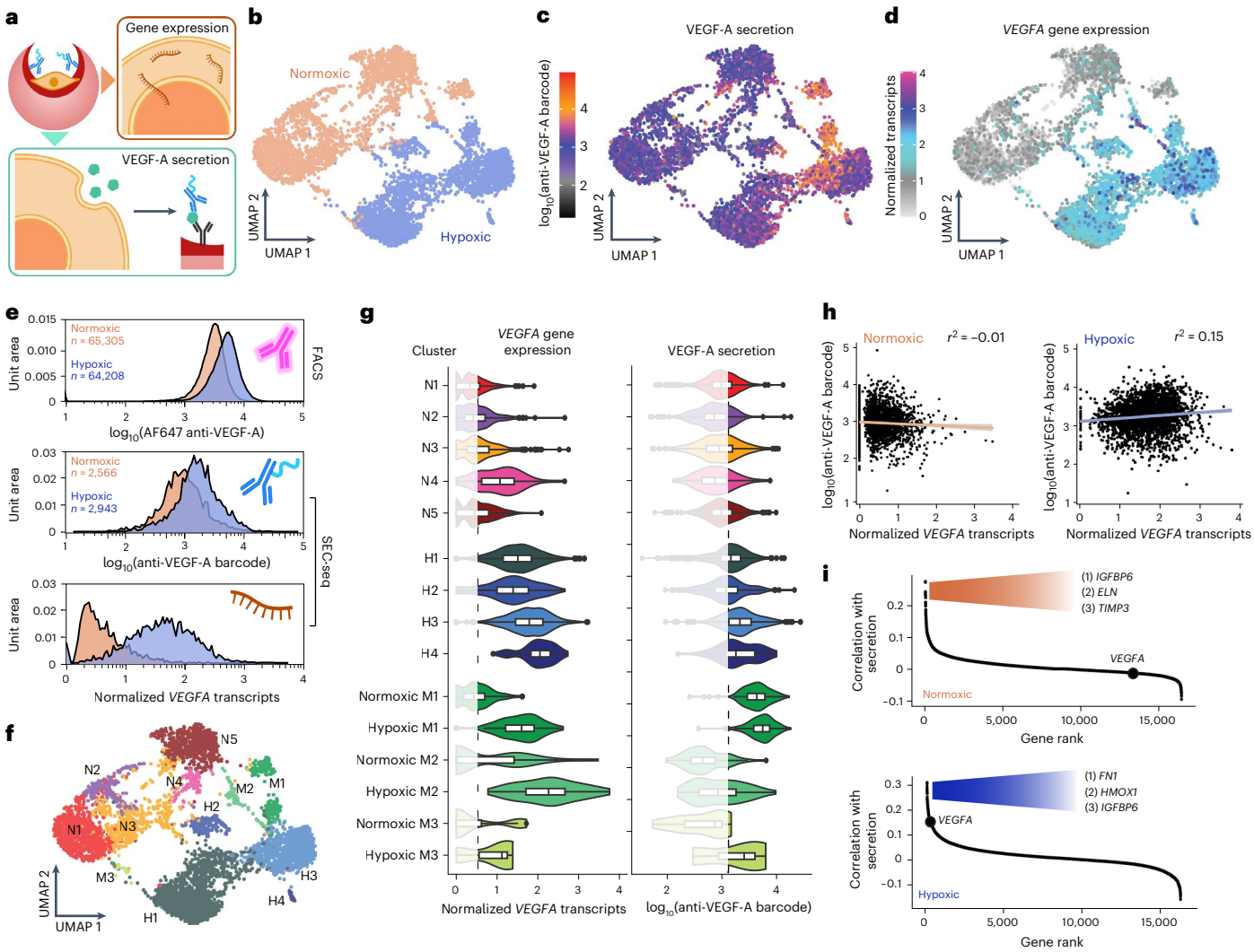

Fig. 3 | SEC-seq measuring the transcriptome and VEGF-A secretion of normoxic or hypoxic MSCs. a, Detection of secreted VEGF-A protein and corresponding global gene expression for individual MSCs using SEC-seq. **b**, UMAP dimensionality reduction based on transcriptomes from SEC-seq experiments on normoxic and hypoxic MSCs in nanovials. Cells are labelled according to the culture condition. $n = 2{,}943$ hypoxic and $n = 2{,}566$ normoxic cells. **c**, UMAP showing VEGF-A secretion level, shown as log transformation of the unique molecular identifier collapsed anti-VEGF-A oligo-barcode reads per cell. **d**, UMAP showing normalized *VEGFA* transcript levels per cell. **e**, Distribution of VEGF-A secretion for cell-loaded nanovials in normoxic and hypoxic conditions, detected by FACS using a fluorescent anti-VEGF-A antibody (top) or by the SEC-seq experiment in **b** using the oligo-barcoded anti-VEGF-A antibody (middle). The bottom plot shows the distribution of *VEGFA* transcript levels from the SEC-seq experiment cells in **b**. **f**, UMAP showing cluster assignment. **g**, Violin plots showing *VEGFA* transcripts and VEGF-A secretion levels for all cells in the normoxic clusters (N1–N5, red shades), hypoxic clusters (H1–H4, blue shades) and mixed clusters (M1–M3, green shades) from **f**. For mixed clusters, the levels are shown separately for normoxic and hypoxic cells. The box plot shows median, quartiles and outliers. The dashed line represents the mean across all cells for each plot. Data below this threshold are lightened to highlight differences. **h**, Scatter plots showing the relationship between *VEGFA* transcript and VEGF-A secretion levels for individual normoxic (left) and hypoxic (right) cells from the experiment in **b**. Best-fit regression lines and Pearson correlation coefficients are shown. **i**, Ranking of all detected genes by the correlation of their transcript levels with the VEGF-A secretion level per cell for normoxic (top) and hypoxic (bottom) MSCs. The rank of the *VEGFA* gene is highlighted, and the top-three genes per sample are noted. Schematics in **a** and **e** created with BioRender.com.

culture conditions (Extended Data Fig. 6a). The hypoxic clusters have higher *VEGFA* transcript and protein secretion levels than the normoxic clusters (Fig. 3g). However, the cluster with the highest minimum and median VEGF-A secretion levels contains cells from both culture conditions (cluster M1) and *VEGFA* transcript levels are not increased in this cluster compared with others (Fig. 3g). These findings confirm the disconnect between VEGF-A secretion, measured over 14 hours, and transcript levels assessed at the endpoint. They also define a unique cell cluster associated with high VEGF-A secretion in both hypoxic and normoxic culture conditions.

To further examine the transcript–secretion relationship, we calculated the correlation between *VEGFA* transcripts and VEGF-A secretion. These features were uncorrelated in normoxic cells ($r^2 = -0.01$) and weakly correlated in hypoxic cells ($r^2 = 0.15$; Fig. 3h). A repeat SEC-seq experiment with normoxic MSCs showed a similar result ($r^2 = 0.05$). When ranking all genes according to the correlation of their transcript levels to VEGF-A secretion, the *VEGFA* transcript ranked lowly in the normoxic cells (rank 13,323; Fig. 3i and Supplementary Table 2). In contrast, *VEGFA* was within the top 2% of correlated genes in hypoxic cells (rank 215; Fig. 3i). Consistent with this, we found a slightly higher transcript–secretion correlation across normoxic and hypoxic cells together ($r^2 = 0.24$; Extended Data Fig. 6b). We conclude that although hypoxia triggers a modest correlation between transcript levels and secretion, the *VEGFA* transcript level at the end of our secretion capture

period has minimal concordance with the VEGF-A secretion amount. This effect is independent of cell depth (Extended Data Fig. 6c).

'Vascular regenerative signal' defines high VEGF-A secretors

As *VEGFA* transcripts were not predictive of secretion, we were interested in a signature that was, especially as the top-correlating genes overlap between normoxic and hypoxic cells (Fig. 4a,b). The top-correlating genes regulate cell growth and migration (*IGFBP5*)[19,20] or have been previously linked to VEGF-A secretion (*IGFBP6*)[11]. Cells in the highly secreting cluster M1 showed the highest transcript levels for these genes (Fig. 4c and Extended Data Fig. 7a). The results were similar in an additional normoxic MSC SEC-seq experiment, where we also found a subpopulation (cluster C5) marked by high VEGF-A secretion and high levels of the top-correlated genes (Fig. 4d,e and Extended Data Fig. 7b–d), which again was not characterized by an increase in *VEGFA* transcript levels. In this repeat, *IGFBP6* was again the top ranked gene when correlating transcript levels of all genes with VEGF-A secretion ($r^2 = 0.48$) and *VEGFA* transcripts lacked correlation with secretion ($r^2 = 0.05$; Extended Data Fig. 7e–h). The highly VEGF-A-secreting cluster could be easily identified even after cell-cycle regression (Extended Data Fig. 8). The high expression of a set of genes reproducibly correlates with the highest VEGF-A secretion in MSCs and suggests that a subpopulation of MSCs with a defined transcriptional state, identified by a specific cluster in each SEC-seq experiment, is reliably linked to highest VEGF-A secretion.

Gene Ontology analysis of differentially expressed genes (Fig. 4e–g and Supplementary Table 3) showed that genes defining the high-VEGF-A-secreting cluster C5 are associated with blood vessel morphogenesis and development, indicative of angiogenesis-related activities and consistent with known VEGF-A function. Surprisingly, similar Gene Ontology terms were found for gene signatures enriched in clusters C6–C10, despite minimal gene overlap (Fig. 4g). Due to overlapping Gene Ontology terms and lack of *VEGFA* transcript correlation, a traditional scRNA-seq analysis would have overlooked cluster C5's identity as a highly VEGF-A secretory subpopulation.

To create a robust gene expression signature marking the high-VEGF-A-secreting MSC subpopulation, we overlapped the differentially expressed genes in the high VEGF-A secretion clusters from three SEC-seq experiments and derived a consensus set of 153 genes (Fig. 4h and Supplementary Table 4). Gene Ontology analysis linked this gene set to matrix organization, cell motility, angiogenesis and wound healing (Fig. 4i), so we coined it the vascular regenerative signal (VRS). The VRS marked a subpopulation composed of 5–20% of the cells loaded in nanovials for our SEC-seq (Fig. 4j) and scRNA-seq experiments (Fig. 4k). VRS-expressing cells were also found in suspended MSC scRNA-seq data (16%; Fig. 4l), demonstrating that the VRS exists independently of possible autocrine and/or substrate effects caused by nanovial containment.

Interestingly, a large proportion of VRS genes classified as secretory genes (29%), much higher than the percentage in all other clusters (Fig. 4m). The VRS includes secretory genes implicated in promoting angiogenesis such as *ELN* and *CXCL12*; *HMOX1*, coding a cryoprotective protein; *FB1*, fibronectin 1, an extracellular matrix glycoprotein involved in tissue repair; *TIMP3*, which helps stabilize the extracellular matrix; and *SCUBE3*, involved in tumour angiogenesis and metastasis[21–26] (Supplementary Table 4). The VRS also includes various cell surface proteins and transcription factors known for their role in mesenchymal fate control such as *KLF6*, *PRRX2* and *RBPJ*[27–29] (Fig. 4m). Using a database that infers regulatory transcription factors for target genes (TRRUST)[30], we found a link between VRS genes and NFKB1, RELA, TFAP2A, ERG and the hypoxia regulator HIF1A (Fig. 4n). VRS genes correlate highly with VEGF-A secretion, with 85% of them within the top-500 correlating genes across all SEC-seq experiments (Fig. 4o). The VRS is a unique gene expression signature that identifies super secretors of VEGF-A, the discovery of which was only made possible by combining the transcriptomic and secretory data of individual cells using SEC-seq. We conclude that VEGF-A secretion by MSCs is regulated by multiple regulatory pathways captured by distinct transcriptional states: cell states broadly increasing basal VEGF-A secretion triggered by hypoxia as well as a specialized subpopulation marked by the VRS signal (Fig. 4p).

Enriching the VRS subpopulation

We hypothesized that VRS genes, which include 19 genes encoding surface proteins (Extended Data Fig. 9a), may be exploited to isolate the high-VEGF-A-secreting MSC subpopulation. We found that an antibody targeting interleukin-13 receptor subunit alpha 2 (IL13RA2), a protein encoded by the third-ranked surface marker gene in the VRS with high transcriptional enrichment (Fig. 5a and Extended Data Fig. 9b), marked a subpopulation of cells with similar frequency to the VRS cells (Fig. 5b; 4–12%). IL13RA2-positive (IL13RA2+) MSCs also had 2.2-times higher mean signal for cell surface protein CD248, which also is included in the VRS, compared with IL13RA2-negative (IL13RA2−) cells (Extended Data Fig. 9a,c).

To explore whether IL13RA2+ cells are enriched for the VRS subpopulation, we isolated IL13RA2+ and IL13RA2− cells by FACS in three replicates and performed bulk RNA sequencing and functional secretion assays. Nearly all VRS genes showed higher expression in IL13RA2+ cells compared with IL13RA2− cells (Fig. 5c and Supplementary Table 5). On average, IL13RA2+ cells had an approximately 2-fold increase in VRS gene expression across the replicates; VRS genes with high VEGF-A secretion–transcript correlation were also highly enriched in IL13RA2+ cells including *IGFBP5* (40-fold higher) and *ELN* (11-fold) (Fig. 5d). *VEGFA* gene expression was not significantly different between both cell populations (Fig. 5c). Genes significantly upregulated in IL13RA2+ cells compared with IL13RA2− cells specifically mark VRS

Fig. 4 | Characterization of the high-VEGF-A-secreting MSC subpopulation. **a**, Scatter plot of VEGF-A secretion–transcript correlation for all genes based on SEC-seq data from normoxic and hypoxic MSCs from Fig. 3 with the ten most highly correlated genes across both experiments labelled. **b**, For the ten top ranked genes from **a**, correlation value in normoxic and hypoxic cells and the average across both. **c**, UMAPs (from the SEC-seq experiment in Fig. 3) showing the VEGF-A secretion levels and expression of five genes from **b** in normoxic and hypoxic MSCs. Cluster M1 is circled. **d**, The same as in **c** for a replicate SEC-seq experiment performed on normoxic MSCs. Cluster 5 is circled. **e**, Cell clustering of the UMAP for the replicate SEC-seq experiment. **f**, Left: heat map of the top-ten differentially expressed genes from each cluster of the SEC-seq experiment in **d** (rows are genes and columns are individual cells). Log-transformed VEGF-A secretion and *VEGFA* transcript levels are shown on top. Right: top-three differentially expressed genes per cluster. **g**, Top Gene Ontology terms found for the differentially expressed genes from the clusters in **e**. The −log*P* value indicates the degree of enrichment for a given cluster. **h**, Venn diagram showing the overlap of differentially expressed genes from the highly secreting cluster in each of three SEC-seq experiments (top left, normoxic MSCs (Fig. 3b); top right, hypoxic MSCs (Fig. 3b); bottom, normoxic MSCs (**e**)). Overlapping genes form the VRS. **i**, Gene Ontology analysis for VRS genes. **j**, Average normalized transcript level of VRS genes per cell for the SEC-seq experiment in **e** and Fig. 3b. **k**, The same as in **j** for MSCs loaded in oligo-barcoded nanovials (Fig. 2j–l). **l**, The same as in **j** for a standard scRNA-seq experiment on unsorted, suspended MSCs. **m**, Gene-type classification for consensus VRS genes versus genes differentially expressed in all clusters in **e**, except C5. **n**, Transcription factor enrichment for VRS genes based on the Transcriptional Regulatory Relationships Unraveled by Sentence-based Text mining (TRRUST) database. **o**, Consensus rank of VEGF-A secretion–transcript correlation based on the SEC-seq experiments in **h**. The red dots indicate VRS genes. **p**, Heterogeneity of VEGF-A secretion in normoxic and hypoxic MSCs, highlighting VRS-associated VEGF-A secretion. Schematic created with BioRender.com.

https://doi.org/10.1038/s41565-023-01560-7

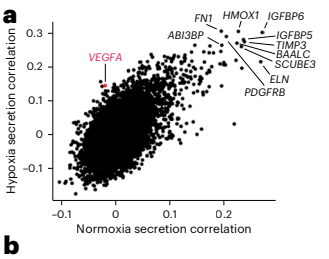

b

Consensus rank	Gene	Normoxia secretion correlation	Hypoxia secretion correlation	Average correlation
1	*IGFBP6*	0.277	0.306	0.292
2	*HMOX1*	0.233	0.309	0.271
3	*IGFBP5*	0.243	0.285	0.264
4	*TIMP3*	0.244	0.279	0.261
5	*FN1*	0.202	0.310	0.256
6	*PDGFRB*	0.211	0.294	0.253
7	*BAALC*	0.231	0.274	0.253
8	*SCUBE3*	0.239	0.264	0.252
9	*ELN*	0.275	0.219	0.247
10	*ABI3BP*	0.202	0.268	0.235

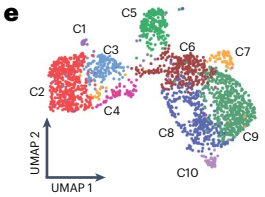

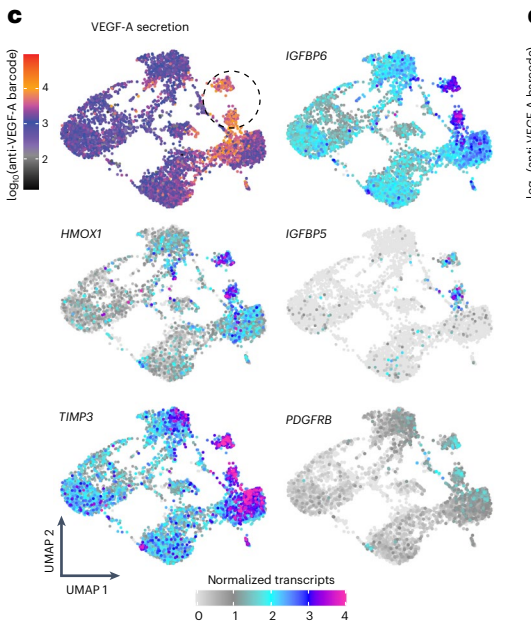

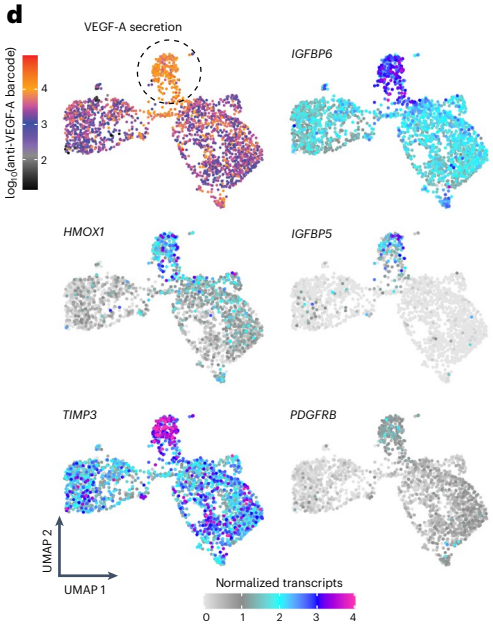

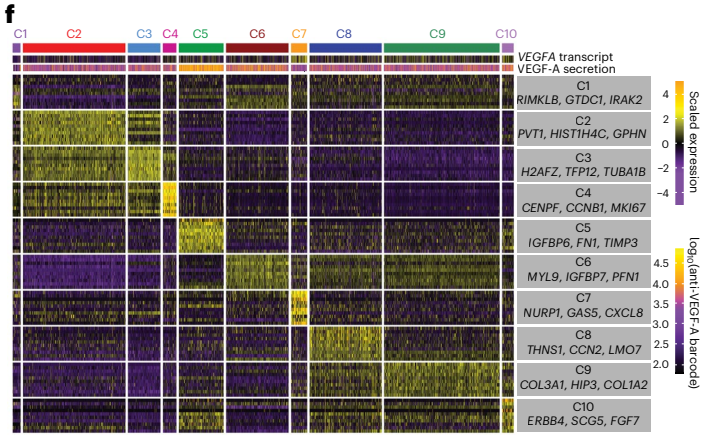

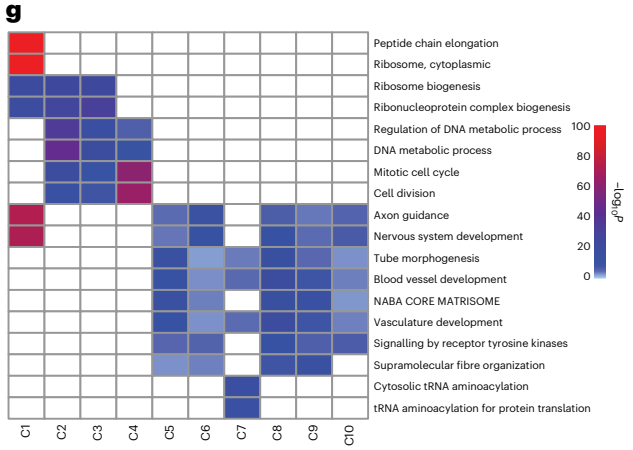

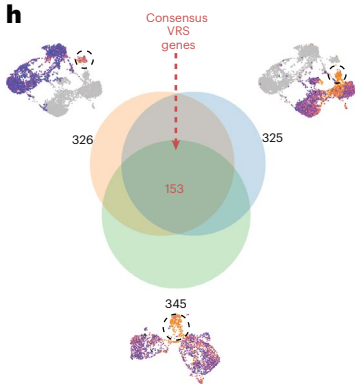

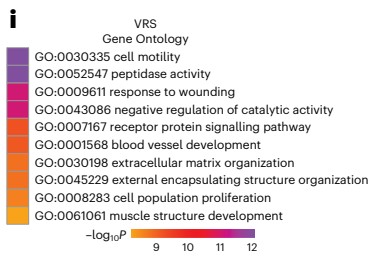

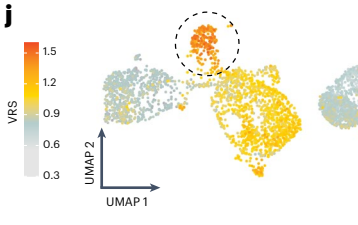

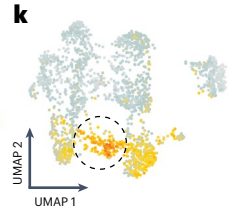

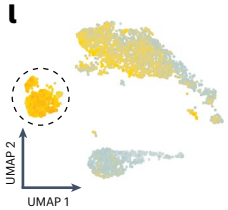

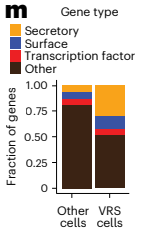

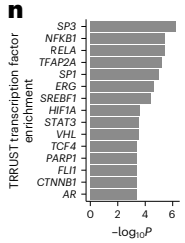

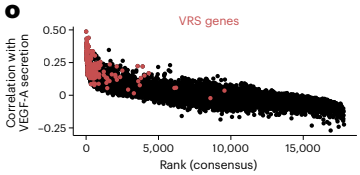

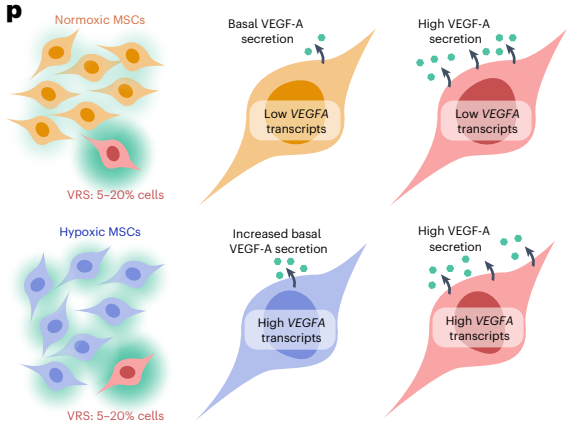

https://doi.org/10.1038/s41565-023-01560-7

cells (Fig. 5e, cluster C5). This indicates that the IL13RA2+ cells capture the gene expression state of the VRS subpopulation of MSCs. The bulk sequencing data allowed us to analyse the splicing pattern of *VEGFA* in IL13RA2+ and IL13RA2− cells (Extended Data Fig. 10a), which revealed no significant splicing difference between the populations, ruling out alternative splicing as a potential source of increased VEGF-A secretion in the VRS subpopulation (Extended Data Fig. 10b,c).

We next asked whether IL13RA2+ cells not only transcriptionally but also functionally recapitulate the VRS population's high VEGF-A secretion. We measured the VEGF-A secretion level from IL13RA2+

Fig. 5 | Enrichment of VRS MSCs using a surface marker identified by SEC-seq. **a**, UMAP from the SEC-seq experiment of normoxic MSCs from Fig. 4d, showing the transcript levels of *IL13RA2*. **b**, Flow cytometry histograms of normoxic MSCs with anti-IL13RA2 labelling and without (negative control). Gates used to sort IL13RA2+ and IL13RA2− cells are shown. APC/Vio 777, Allophycocyanin/Vio® 770. **c**, Volcano plot showing the average $\log_2$(fold change) in transcript levels per gene between IL13RA2+ and IL13RA2− cells from triplicate bulk RNA-seq experiments and −log*P* which represents the significance of the difference between the two sample groups. Significant genes are highlighted in black (threshold >1.5 $\log_2$ fold change, $P < 0.05$), VRS genes are labelled in pink and *VEGFA* is labelled in green. **d**, Heat map showing the row-normalized transcript levels of the top-20 VEGF-A secretion correlates from the experiment in Fig. 4b, which include many VRS genes, for the three bulk RNA-seq replicates for IL13RA2+ and IL13RA2− cells. **e**, UMAP from the SEC-seq experiment of normoxic MSCs from Fig. 4d showing the average transcript levels of genes significantly upregulated in IL13RA2+ compared with IL13RA2− cells (>4-fold change, $P < 0.05$). **f**, VEGF-A ELISpot assay spot count for MSCs (IL13RA2+ and IL13RA2−) sorted immediately after isolation by FACS. Data are presented as mean values ± s.d. for three replicate wells. **, $P < 0.01$. **g**, VEGF-A secretion measured by ELISA from conditioned media taken from IL13RA2+ and IL13RA2− cells expanded for 6 days after sort. Data presented as mean values ± s.d. for two expanded replicates. *, $P < 0.05$. **h**, Top: flow cytometry histogram plot of normoxic MSCs stained for IL13RA2. Bottom: flow cytometry histograms for the IL13RA2+ and IL13RA2− populations after expansion for 6 days. **i**, Workflow leveraging SEC-seq data for isolation of a subpopulation of interest. Schematic created with BioRender.com.

and IL13RA2− cells isolated by FACS using a VEGF-A ELISpot assay and found that IL13RA2+ cells produced 30% more spots than the IL13RA2− samples ($P < 0.05$; Fig. 5f). In parallel, isolated IL13RA2+ and IL13RA2− cells were expanded in culture, and then retested for IL13RA2 staining by flow cytometry. After 6 days of culture, 81.4% of the IL13RA2+ cells retained high IL13RA2 levels above the threshold and expanded IL13RA2− cells remained negative for this marker (Fig. 5h). In a repeat experiment, we measured VEGF-A levels by enzyme-linked immunosorbent assay (ELISA in conditioned media obtained from IL13RA2+ and IL13RA2− expanded cells and found that VEGF-A secretion was 1.6-fold higher in the IL13RA2+ population following expansion (Fig. 5g and Extended Data Fig. 9d). These data corroborate the technical accuracy of SEC-seq to measure secretion and shows that the enriched VRS population maintains higher VEGF-A secretion and can be expanded for downstream assays. Using SEC-seq, we can characterize and identify cell subsets with unique secretory characteristics and the data can also be leveraged to enrich populations for expansion in applications where increased VEGF-A secretion is desirable (Fig. 5i).

Discussion

Developing and using SEC-seq, we linked the secretion function of ~10,000 single MSCs to their transcriptomes. Our work studied secretion in adherent cells, but suspension cells are also compatible with SEC-seq[31]. Previously, simultaneous measurements of cell-associated proteins and transcriptome could be performed, but methods to detect secretions and transcriptome were inaccessible. Cellular indexing of transcriptomes and epitopes by sequencing (CITE-seq) detects cell surface proteins with the cell's transcriptome[9,32], which facilitated the discovery of markers specific for activated regulatory T cells and highly functional stem cells[33,34]. We anticipate that SEC-seq will open a similar dimension of exploration for secreted proteins. A recent method, TRAPS-seq, reported simultaneous measurement of transcriptome and secretions of leukocytes via affinity matrices on the cell surface[35]; however, using the dynamic cell membrane for secretion capture limits potential applications, flexibility and accuracy of the measurement.

Our data uncover the high level of heterogeneity in secretion of VEGF-A in MSCs under normoxic and hypoxic conditions, and reveals new transcriptionally defined subpopulations such as the VRS-marked cells, only uncovered using SEC-seq. Other studies have also described similar functional subpopulations in MSCs[36,37], some which also show high expression of VRS genes[38,39]. As the primary mechanism of action for MSC therapies is thought to be through the secretion of bioactive factors that promote immunomodulation and regeneration, such as VEGF-A, the VRS could provide a foundation for developing critical quality attributes for MSC therapies. Notably, the VRS provides genes and pathways that could be genetically targeted or modified by pre-conditioning treatments and candidate surface marker genes that could be used for isolation of high-secreting subpopulations. This was shown using IL13RA2 as a marker of VRS cells, which maintained their gene expression and secretory characteristics for several population doublings.

Transcriptional expression of a secretory protein is often equated to secretion; however, our results indicate that this assumption may not always be correct. We found that *VEGFA* transcripts and VEGF-A secretion have very low correlation in normoxic and hypoxic MSCs. While surprising, the uncoupling of transcript level and protein secretion is aligned with studies using CITE-seq where certain surface protein and transcripts feature low correlation[9,10,40]. This opens new questions, including (1) how dependent is secretion on cell state; (2) how are cells facilitating the build-up and release of secreted protein outside of gene regulation; and (3) why would the uncoupling of secretion and transcript levels be beneficial compared with direct control of secretion via the transcript regulation. Our results suggest that driving secretion for engineered cell therapy functions[41] should not rely alone on increasing the transcript level of the target gene, but could benefit from holistic engineering of the pathways involved in secretion.

We acknowledge limitations in the SEC-seq assay. Currently, SEC-seq requires cells with diameters less than 20 µm to fit in 35 µm nanovials. There is an inherent temporal mismatch between the cell's messenger RNA detected at the instant of lysis and the gradual secreted protein accumulating over the length of the cell's time in the nanovial. In this study, we characterized only a single secreted protein, although multiplexing secreted proteins using SEC-seq should be possible.

Using SEC-seq, we can answer critical questions about the secretome, including which cells secrete specific proteins, whether there is coordinated secretion among proteins and what mechanisms control secretion. Extending the boundaries of multiomics, SEC-seq democratizes the ability to make discoveries by linking cell secretion with gene expression for thousands of cells using nanovial technology.

Online content

Any methods, additional references, Nature Portfolio reporting summaries, source data, extended data, supplementary information, acknowledgements, peer review information; details of author contributions and competing interests; and statements of data and code availability are available at https://doi.org/10.1038/s41565-023-01560-7.

References

1. Uhlén, M. et al. Tissue-based map of the human proteome. *Science* **347**, 1260419–1260419 (2015).
2. Miwa, H., Dimatteo, R., de Rutte, J., Ghosh, R. & Di Carlo, D. Single-cell sorting based on secreted products for functionally defined cell therapies. *Microsyst. Nanoeng.* **8**, 84 (2022).
3. Levy, O. et al. Shattering barriers toward clinically meaningful MSC therapies. *Sci. Adv.* **6**, eaba6884 (2020).
4. Kode, J. A., Mukherjee, S., Joglekar, M. V. & Hardikar, A. A. Mesenchymal stem cells: immunobiology and role in immunomodulation and tissue regeneration. *Cytotherapy* **11**, 377–391 (2009).
5. Bode, D., Cull, A. H., Rubio-Lara, J. A. & Kent, D. G. Exploiting single-cell tools in gene and cell therapy. *Front. Immunol.* **12**, 2775 (2021).

6. Lee, S., De Rutte, J., Dimatteo, R., Koo, D. & Di Carlo, D. Scalable fabrication and use of 3D structured microparticles spatially functionalized with biomolecules. *ACS Nano* **16**, 38–49 (2022).
7. De Rutte, J. et al. Suspendable hydrogel nanovials for massively parallel single-cell functional analysis and sorting. *ACS Nano* **16**, 7242–7257 (2022).
8. de Rutte, J., Dimatteo, R., Zhu, S., Archang, M. M. & Di Carlo, D. Sorting single-cell microcarriers using commercial flow cytometers. *SLAS Technol.* **27**, 150–159 (2022).
9. Stoeckius, M. et al. Simultaneous epitope and transcriptome measurement in single cells. *Nat. Methods* **14**, 865–868 (2017).
10. Peterson, V. M. et al. Multiplexed quantification of proteins and transcripts in single cells. *Nat. Biotechnol.* **35**, 936–939 (2017).
11. Thej, C., Ramadasse, B., Walvekar, A., Majumdar, A. S. & Balasubramanian, S. Development of a surrogate potency assay to determine the angiogenic activity of Stempeucel®, a pooled, ex-vivo expanded, allogeneic human bone marrow mesenchymal stromal cell product. *Stem Cell. Res. Ther.* **8**, 1–14 (2017).
12. Berry, J. D. et al. NurOwn, phase 2, randomized, clinical trial in patients with ALS. *Neurology* **93**, e2294–e2305 (2019).
13. Yousefi, K. et al. The design and rationale of a phase 2b, randomized, double-blinded, and placebo-controlled trial to evaluate the safety and efficacy of lomecel-B in older adults with frailty. *J. Frailty Aging* **11**, 214–223 (2022).
14. Mereu, E. et al. Benchmarking single-cell RNA-sequencing protocols for cell atlas projects. *Nat. Biotechnol.* **38**, 747–755 (2020).
15. Koch, F. et al. Generic method of printing window adjustment for extrusion-based 3D-bioprinting to maintain high viability of mesenchymal stem cells in an alginate-gelatin hydrogel. *Bioprinting* **20**, e00094 (2020).
16. Schwartz, M. A. & Assoian, R. K. Integrins and cell proliferationregulation of cyclin-dependent kinases via cytoplasmic signaling pathways. *J. Cell Sci.* **114**, 2553–2560 (2001).
17. Potier, E. et al. Hypoxia affects mesenchymal stromal cell osteogenic differentiation and angiogenic factor expression. *Bone* **40**, 1078–1087 (2007).
18. Liu, G.-S. et al. Pharmacological priming of adipose-derived stem cells for paracrine VEGF production with deferoxamine. *J. Tissue Eng. Regen. Med.* **10**, E167–E176 (2016).
19. Waters, J. A., Urbano, I., Robinson, M. & House, C. D. Insulin-like growth factor binding protein 5: diverse roles in cancer. *Front. Oncol.* **12**, 1052457 (2022).
20. Sureshbabu, A. et al. IGFBP5 induces cell adhesion, increases cell survival and inhibits cell migration in MCF-7 human breast cancer cells. *J. Cell Sci.* **125**, 1693–1705 (2012).
21. Al Halawani, A., Abdulkhalek, L., Mithieux, S. M. & Weiss, A. S. Tropoelastin promotes the formation of dense, interconnected endothelial networks. *Biomolecules* **11**, 1318 (2021).
22. Zheng, H., Fu, G., Dai, T. & Huang, H. Migration of endothelial progenitor cells mediated by stromal cell-derived factor-1alpha/CXCR4 via PI3K/Akt/eNOS signal transduction pathway. *J. Cardiovasc. Pharmacol.* **50**, 274–280 (2007).
23. Chou, C. H. et al. SCUBE3 regulation of early lung cancer angiogenesis and metastatic progression. *Clin. Exp. Metastasis* **30**, 741–752 (2013).
24. Fan, D. & Kassiri, Z. Biology of tissue inhibitor of metalloproteinase 3 (TIMP3), and its therapeutic implications in cardiovascular pathology. *Front. Physiol.* **11**, 661 (2020).
25. Poss, K. D. & Tonegawa, S. Heme oxygenase 1 is required for mammalian iron reutilization. *Proc. Natl Acad. Sci. USA* **94**, 10919 (1997).
26. Lenselink, E. A. Role of fibronectin in normal wound healing. *Int. Wound J.* **12**, 313 (2015).
27. DiFeo, A., Martignetti, J. A. & Narla, G. The role of KLF6 and its splice variants in cancer therapy. *Drug Resist. Updat.* **12**, 1–7 (2009).
28. Higuchi, M. et al. PRRX1- and PRRX2-positive mesenchymal stem/progenitor cells are involved in vasculogenesis during rat embryonic pituitary development. *Cell Tissue Res.* **361**, 557–565 (2015).
29. Dong, Y. et al. RBPjkappa-dependent Notch signaling regulates mesenchymal progenitor cell proliferation and differentiation during skeletal development. *Development* **137**, 1461–1471 (2010).
30. Han, H. et al. TRRUST v2: an expanded reference database of human and mouse transcriptional regulatory interactions. *Nucleic Acids Res.* **46**, D380–D386 (2018).
31. Cheng, R. Y.-H. et al. SEC-seq: association of molecular signatures with antibody secretion in thousands of single human plasma cells. *Nat. Commun.* **14**, 3567 (2023).
32. Shum, E. Y., Walczak, E. M., Chang, C. & Christina Fan, H. Quantitation of mRNA transcripts and proteins using the BD Rhapsody™ single-cell analysis system. *Adv. Exp. Med. Biol.* **1129**, 63–79 (2019).
33. Trzupek, D. et al. Discovery of CD80 and CD86 as recent activation markers on regulatory T cells by protein-RNA single-cell analysis. *Genome Med.* **12**, 55 (2020).
34. Vanuytsel, K. et al. Multi-modal profiling of human fetal liver hematopoietic stem cells reveals the molecular signature of engraftment. *Nat. Commun.* **13**, 1103 (2022).
35. Wu, T. et al. Time-resolved assessment of single-cell protein secretion by sequencing. *Nat. Methods* **20**, 723–734 (2023).
36. Xie, Z. et al. Single-cell RNA sequencing analysis of human bone-marrow-derived mesenchymal stem cells and functional subpopulation identification. *Exp. Mol. Med.* **54**, 483–492 (2022).
37. Sun, C. et al. Single-cell RNA-seq highlights heterogeneity in human primary Wharton's jelly mesenchymal stem/stromal cells cultured in vitro. *Stem Cell Res. Ther.* **11**, 149 (2020).
38. Zhang, C. et al. Single-cell transcriptomic analysis reveals the cellular heterogeneity of mesenchymal stem cells. *Genomics Proteom. Bioinform.* **20**, 70–86 (2022).
39. Cui, Y. et al. Single-cell characterization of monolayer cultured human dental pulp stem cells with enhanced differentiation capacity. *Int. J. Oral. Sci.* **13**, 44 (2021).
40. Vistain, L. et al. Quantification of extracellular proteins, protein complexes and mRNAs in single cells by proximity sequencing. *Nat. Methods* **19**, 1578–1589 (2022).
41. Baloh, R. H. et al. Transplantation of human neural progenitor cells secreting GDNF into the spinal cord of patients with ALS: a phase 1/2a trial. *Nat. Med.* **28**, 1813–1822 (2022).

Methods

MSC cell culture

Immortalized human adipose-derived MSCs (ATCC SCRC-4000) were cultured in MSC basal medium (ATCC PCS-500-030) supplemented with low-serum MSC growth kit for adipose MSCs (ATCC PCS-500-040) and antibiotic-antimycotic (Invitrogen), resulting in final complete MSC media concentrations of 2% fetal bovine serum (FBS), 5 ng ml^{-1} FGF-1, 5 ng ml^{-1} FGF-2, 5 ng ml^{-1} EGF, 2.4 mM L-alanyl-L-glutamine and 1% antibiotic-antimycotic. MSCs were cultured in incubators at 37 °C and 5% CO_2 and passaged once 70–80% confluent, with MSCs up to passage 25 used in experiments.

Nanovial fabrication and modifications

See Fig. 1b for schematic and images during fabrication. The 35 µm nanovials were fabricated using a three-inlet flow-focusing microfluidic device formed from polydimethylsiloxane. Polyethylene glycol (PEG) pre-polymer, gelatin and oil phases were infused at flow rates of 1.5 µ min^{-1}, 1.5 µl min^{-1} and 15 µl min^{-1}, respectively. The PEG pre-polymer phase comprised 27.5% w/v 5 kDa four-arm PEG acrylate (Advanced BioChemicals) with 4% w/v lithium phenyl-2,4,6-trimethylbenzoylphosphinate (Sigma) in PBS (pH 7.2). The gelatin phase comprised 20% w/v cold water fish gelatin (Sigma) in deionized water. The oil phase comprised Novec 7500 (3 M) with 0.5% v/v Pico-surf (Sphere Fluidics). Oil partitioned the aqueous phases into monodisperse water-in-oil droplets and the PEG and gelatin polymers phase separated into PEG-rich and gelatin-rich phases. Phase-separated droplets were crosslinked with focused ultraviolet light through a DAPI filter set and 10x microscope objective (Nikon, Eclipse Ti-S) near the outlet region of the microfluidic device. Polymerized nanovials were collected and any unreacted phases including oil were removed through a series of washing steps as previously described[6,7]. Biotinylation of the gelatin layer formed in the nanovial cavity was conducted by incubating nanovials with 10 mM sulfo-NHS-biotin (APExBIO) overnight at room temperature while mixing. Nanovials were then washed in pluronic buffer consisting of 0.05% pluronic F-127 (Sigma), 1% antibiotic-antimycotic (Thermo Fisher) in PBS and sterilized in 70% ethanol overnight. Sterile nanovials were stored 5-times diluted (that is, 100 µl of concentrated nanovial volume was resuspended in 400 µl pluronic buffer resulting in 6.5 million nanovials per ml) in this pluronic buffer at 4 °C.

Conjugating VEGF-A capture antibodies to nanovials

Five-times diluted nanovial suspension was incubated with an equal volume of 260 µg ml^{-1} of streptavidin for 30 min at room temperature on a tube rotator. Excess streptavidin was washed out by pelleting nanovials at 200*g* for 3–5 min, removing supernatant and adding 1 ml of wash buffer (pluronic buffer + 0.5% bovine serum albumin) three times. All subsequent wash steps in assay workflows were performed similarly unless otherwise noted. The 5-times diluted streptavidin-coated nanovial suspension was then incubated with an equal volume of 71.5 µg ml^{-1} of biotinylated human VEGF antibody (BioLegend) for 30 min at room temperature on a tube rotator and washed. Nanovials were resuspended at a five-times dilution in wash buffer or cell culture medium before the next workflow step.

Loading cells in nanovials

MSCs were loaded into nanovials by pipette-mixing nanovials and the cell solution in 5 ml round-bottom polypropylene tubes (Corning Falcon), which provide a cell-adhesion resistant material and vent cap for gas exchange during incubation. First, the five-times diluted nanovial suspension was reconstituted in complete MSC media. MSCs were detached from tissue culture flasks using TrypLE (Gibco) and resuspended in media at concentrations of 0.9, 1.5 and 2.2 million per ml. Cells and nanovials are then pipette-mixed 10 times in a 3:1 volume ratio for final cell-to-nanovial ratios of 0.4:1, 0.7:1 and 1:1, respectively. A total volume of less than 0.5 ml per tube was maintained throughout to reduce cell clumping during incubation. The nanovial suspensions were incubated at 37 °C and 5% CO_2 for 2 h to allow MSCs to bind to the gelatin coating in nanovial cavities. Then nanovial suspensions were first strained through a 20 µm strainer (CellTrics) to remove unbound cells. Subsequently, recovered nanovials were strained through a 37 µm strainer (STEMCELL) to remove any large-cell/nanovial aggregates. The 1:1 cell-to-nanovial ratio was used for remaining experiments.

Single-cell VEGF-A secretion on nanovials

VEGF-A capture antibody-conjugated nanovials were loaded with MSCs as described above. After straining, nanovials were incubated in 6-well plates for 12 h, in addition to 2 h loading, to allow for secretion, with up to 170,000 nanovials per well in 2 ml media (for time sweep secretion experiments total times of 2 h, 8 h and 14 h incubations were performed). Plates were shaken in horizontal cross-movements before placing in the incubator to space out the nanovials. After incubation, nanovials were collected in wash buffer, centrifuged and resuspended as five-times diluted nanovial suspension. This suspension was incubated with an equal volume of 71.5 µg ml^{-1} AF647 human VEGF antibody (Sigma) diluted in a buffer containing calcein AM for 30 min at 37 °C with gentle vortexing every 10 min before washing excess antibody with 1 high-dilution wash (>100 times nanovial volume). Samples were then analysed by imaging using fluorescence microscopy and analysed/sorted by FACS as described below. For the hypoxia inducer concentration sweep, MSCs in nanovials were incubated in cell culture media for the normoxic condition and media supplemented with deferoxamine (100 µM, 250 µM, 500 µM, 1,000 µM) or cobalt chloride (50 µM and 100 µM) for hypoxic conditions. At least 10,000 single-cell-loaded nanovials were analysed per condition.

Flow cytometry and sorting of nanovials using SONY SH800S

Nanovial samples were diluted 25 times in washing buffer before sorting on the SONY SH800S cell sorter using a 130 µm sorting chip. The sorter featured violet (405 nm), blue (488 nm), yellow (561 nm) and red (640 nm) lasers and 450/50 nm (FL1), 525/50 nm (FL2), 600/60 nm (FL3) and 665/30 nm (FL4) filters were used. Typical sensor gain settings used for nanovial samples are given in Table 1, along with stains or antibodies measured using the filters. Compensation was performed for samples with spectral overlap (for example, calcein spillover into FL4 for samples labelled with calcein and AF647 anti-VEGF) using an unstained control (plain nanovials) and single-stained controls (calcein-stained cells on nanovials; AF647 anti-VEGF-A-labelled recombinant VEGF in empty nanovials). The typical gating strategy for nanovials is shown in Supplementary Fig. 1e. Flow cytometry data were analysed using FlowJo software version 10.8 (BD).

Dynamic range of VEGF-A immunoassay on nanovials using flow cytometry

Nanovials were conjugated with biotinylated anti-VEGF-A capture antibody as mentioned earlier. Five-times diluted nanovials were incubated with equal volumes of 0, 0.1, 1, 10, 100, 1,000, 10,000 ng ml^{-1} of recombinant human VEGF-A (R&D Systems) for 12 h at 4 °C on a tube rotator. Excess recombinant VEGF-A was washed before reconstituting as 5-times dilution of nanovials and incubating with equal volume of 71.5 µg ml^{-1} AF647 anti-VEGF-A (BioLegend) at room temperature for 30 min in the dark on a tube rotator. After washing, nanovials were reconstituted as 25-times diluted suspension in wash buffer and transferred to a flow tube. In addition, a small fraction of the sample was transferred to a 96-well plate to be imaged on a fluorescence microscope. The fluorescence signal on nanovials was analysed using the Sony sorter by gating for single particles. To generate the standard curve, the mean signal from each concentration of VEGF-A was calculated on FlowJo and plotted against concentration. This and all other thresholds in this paper are calculated as mean (0 ng ml^{-1} sample) + 2.5 × s.d. (0 ng ml^{-1} sample).

Oligo-barcoded anti-VEGF-A immunoassay validation

To validate the oligo-barcoded anti-VEGF-A specificity on nanovials, we prepared nanovials either with or without recombinant VEGF-A bound (as discussed above, using 1,000 ng ml^{-1} VEGF-A concentration). Then we incubated 5-times diluted nanovials with an equal volume of either 0 or 71.5 ng ml^{-1} oligo-barcoded anti-VEGF-A (BioLegend) for 30 min at room temperature on a tube rotator. The four resulting samples were as follows: (1) VEGF-A$^+$, anti-VEGF-A$^+$, (2) VEGF-A$^-$, anti-VEGF-A$^+$, (3) VEGF-A$^+$, anti-VEGF-A– and (4) VEGF-A–, anti-VEGF-A$^-$. To measure the binding of the oligo-barcoded anti-VEGF-A detection antibodies, we then incubated the 4 samples with an equal volume of 71.5 ng ml^{-1} of AF647 goat anti-mouse IgG (Jackson ImmunoResearch), which binds to the oligo-barcoded anti-VEGF-A antibody that is mouse species, for 30 min at room temperature on a tube rotator. Samples were then analysed on the Sony sorter by gating for single particles.

Single-cell gene expression and feature barcode detection library generation for cell-loaded nanovials

We followed the standard protocol for the Chromium Next GEM Single Cell 3′ Kit v3.1 unless otherwise noted in the methods (10x Genomics, https://www.10xgenomics.com/products/single-cell/). Single-cell-containing nanovials were isolated using FACS, as noted above. Nanovials were prepared in PBS + 0.04% bovine serum albumin at a typical concentration of 500 nanovials per µl (experiments in Fig. 2h,j were done at higher concentrations of 2,000 per µl). We loaded 16.5 µl of this solution containing approximately 8,250 nanovials (target cell recovery ~5,000 cells) into Chip G microfluidic emulsion devices. As nanovials settle more quickly than cells, we adjusted the loading procedure to reduce the time in between sample loading and emulsion generation. During the sample loading step, the nanovial + master mix suspension was first allowed to settle for 2 min after mixing, then the first half (35 µl) was taken from the supernatant and loaded in the 10x chip sample well (row 1). The gel bead well and partitioning oil wells were then loaded. The second half of the nanovial sample (35 µl) was pipette-mixed and added to row 1 immediately before loading into a 10x Chromium controller to generate emulsions. After sequencing, we recovered approximately 40–50% of the target cell recovery number with this method, or ~2,500 nanovials containing cells per experiment.

Libraries were assembled from emulsions according to the protocol (Chromium Single Cell 3′ Reagent Kits User Guide (v3.1 Chemistry Dual Index) with Feature Barcoding technology for Cell Surface Protein and Cell Multiplexing), using the Chromium Single-Cell 3′ Library Kit (10x Genomics) for purification, amplification, fragmentation, end repair, A-tailing, adapter ligation, and final library indexing and amplification. Library clean-up was done with solid-phase reversible immobilization select reagent beads (Beckman Coulter, B23317). Separate libraries were made to detect the nanovial-associated streptavidin oligonucleotide barcode DNA and SEC-seq antibody-conjugated oligonucleotide DNA per cell using the protocol for Cell Surface Protein libraries in the above user guide. All libraries were quantified on a Tapestation 4200 (Agilent, G2991BA) according to the manufacturer's protocols using the D5000 screentape and reagents for complementary DNA quality control (Agilent, 5067-5588, 5067-5589) and D1000 screentape and reagents for final library quality control (Agilent, 5067-5582, 5067-5583). Libraries were pooled and paired-end sequenced at 100 bp per end with an additional 10 bp of index reads on a NovaSeq S4 flow cell (Illumina, Novaseq 6000).

Species mixing experiment

Nanovials were separately loaded with either human MSCs (1 cell:1 nanovial) or mouse embryonic fibroblasts (0.4 cell:1 nanovial). Single-cell-loaded nanovials for each species were separately sorted and then combined in a 1:1 ratio. The sample was reconstituted as 2,000 nanovials per µl before loading into a 10x chip for single-cell sequencing library preparation.

Comparing transcriptomes of suspended cells and cells on nanovials

MSCs were prepared either suspended or loaded in nanovials. The nanovial sample was incubated for 12 h, similar to secretion assay experiments, and labelled with oligo-barcoded streptavidin (BioLegend) after loading. Suspended cells and nanovial samples were sorted for single cells or single cells on nanovials, respectively. An additional sample of suspended cells was left unsorted. Each of the three samples (suspended and sorted, suspended and unsorted, and cells on nanovials) was reconstituted as 500 cells per µl or nanovials per µl and loaded in separate 10x chip channels for single-cell sequencing library preparation.

Barcoded normoxic and hypoxic conditioned MSCs on nanovials pooled for scRNA-seq

MSCs were loaded into nanovials and were incubated for 12 h in either normoxic or hypoxic (500 µM deferoxamine) media. After incubation, each nanovial sample was conjugated with a different oligo-barcoded streptavidin (BioLegend). Nanovial samples were then sorted using the sorting gate for single cells on nanovials, and then normoxic and hypoxic cell-loaded nanovials were combined in a 1:1 ratio. The pooled sample was reconstituted as 1,000 nanovials per µl before loading into a 10x chip for single-cell sequencing library preparation.

SEC-seq for MSC transcriptome and VEGF-A secretion

VEGF-A capture antibody-conjugated nanovials were loaded with MSCs as described above. After straining, nanovials were incubated in 6-well plates for 12 h to accumulate VEGF-A secretions, with up to 170,000 nanovials per well in 2 ml media (cell culture media for the normoxic condition and media supplemented with 500 µM deferoxamine for the hypoxia-inducing condition). Plates were shaken in horizontal cross-movements before placing in the incubator to space out nanovials. After incubation, nanovials were collected in wash buffer, centrifuged and resuspended as five-times-diluted nanovial suspension. This suspension was incubated with an equal volume of 71.5 µg ml^{-1} of oligo-barcoded anti-VEGF-A detection antibody (BioLegend) diluted in a buffer containing calcein AM for 30 min at 37 °C with gentle vortexing every 10 min before washing excess antibody with 1 high-dilution wash (>100× nanovial volume). Samples were then sorted using the SONY SH800S using the single cell on nanovial gate. The normoxic and hypoxic MSCs on nanovial samples were then reconstituted separately as 500 nanovials per µl before loading into a 10x chip for single-cell sequencing library preparation.

Single-cell-sequencing data analysis

Sequencing data were demultiplexed in Basespace and mapped, barcode collapsed and filtered in the Cell Ranger software (10x Genomics). Reads were mapped to the hg38 Refseq human reference transcriptome, or for the mixed species experiment, a fusion of the hg38 genome and the mouse mm38 genome built using the Cell Ranger mkref function. The output from Cell Ranger, a raw sparse matrix with digital expression of cell barcodes by genes, was used for downstream analysis. Species identity was called by mapping to a joined genome contig and determining the ratio of reads from each species' genome.

Using Seurat 4.1 in R (https://github.com/satijalab/seurat), we performed normalization of transcripts and clustering of cells, and obtained reduced dimensionality principal component analysis and UMAP coordinates for each cell. Cells were regressed using depth as the variable. To identify and remove doublets, the cell matrix was processed by DoubletFinder (https://github.com/chris-mcginnis-ucsf/DoubletFinder).

We used streptavidin barcodes linked to nanovials to separate mixed hypoxic and normoxic MSCs in Fig. 2. Barcode reads for this feature were matched to each cell using Cell Ranger's multi-config workflow. We added a pseudocount to each barcode read and, for

each cell, calculated the ratio of barcodes. Cells with a ratio favouring one barcode at least 2.5-fold were called for that tagged sample ('normoxic' or 'hypoxic'), while cells with ratios below 2.5-fold were considered 'mixed' and removed from the analysis. Cells with less than 25,000 streptavidin reads for either sample (~15% of maximum) were considered unannotated and also discarded. In Supplementary Fig. 3, we identified cell separation from nanovials during emulsion formation using detection of a single barcode; here escaped cells were called that had fewer than 800 barcode reads (25% of average read number).

Analysis and plots were mostly created using R and the libraries ggplot2 and pheatmap. The hypoxic gene signature shown in Fig. 2l was derived de novo using the gene–gene correlation method GEND, as previously described[42]. Cell clusters were derived using Seurat's FindNeighbors and FindClusters function, and differential expression among clusters was determined by using the FindMarkers function. Differential expression between samples was determined by testing each gene for a distribution *P* value of less than 0.05 and a fold change greater than 2 between the average gene value in the cells for each sample. Histograms for sequencing data was generated by grouping normalized reads into 100 equally sized bins. Gene Ontology for various gene lists was determined using Metascape (filtered the output for Gene Ontology terns only). Similar Gene Ontology terms were collapsed for Fig. 4i.

Cell-cycle regression was performed using Seurat. Briefly, cell-cycle genes marking S phase and G2/M phases were used to create cell-cycle scores for each cell using the CellCycleScores function. These scores were used to adjust the gene by cell matrix using the ScaleData function to regress out the effect of cell cycle, and then the output was processed and analysed using normal parameters.

SEC-seq reads were recovered from the Cell Surface Protein library workflow and matched to the transcriptome cell barcodes using Cell Ranger's multi-config tag workflow. Secretion reads were log-transformed to more closely match the dynamic range of the normalized gene transcripts. Gene correlates were determined using Pearson's correlation of all gene transcripts against the log of secretion reads. Secretion correlate genes were ranked by order of correlation. For generation of a consensus ordering between multiple SEC-seq experiments, Pearson's correlation values were averaged for each gene and a new ordering rank was determined from that average.

The VRS was determined by identifying the cluster with high *IGFBP6* expression in three MSC scRNA-seq experiments (two normoxic replicates and a hypoxic MSC run), running differential gene expression analysis for the respective cluster against all other cells in the given experiment, and then taking the overlap of genes between the three samples. The per cent of cells in each experiment called 'VRS expressing' was calculated by averaging the expression of all genes in the VRS per cell and using a threshold of 75% of the maximum averaged value. Potential regulators of the VRS genes were determined by testing the VRS genes for enrichments in the TRRUST database[30]. VRS gene types were annotated using separate databases for the secretome (SPRomeDB)[43], transcription factors (ATFDB)[44] and surfactome (SURFY)[45], after overlaps between the secretome and the other two databases were pruned.

Statistics and reproducibility

All experiments were performed at least twice to ensure reproducibility. We tested the VEGF-A SEC-seq protocol three times independently, and found consistent outputs as described in 'Results'. Violins and box plots show all data, with median and quartiles marked. Differential expression was tested using the Wilcoxon ranked sum test and significance was assigned to $P < 0.05$. Exon inclusion probability was tested using the Simes method and significance was assigned to $P < 0.05$ and a false discovery rate <0.10.

See Supplementary Information for a reagents table and additional methods.

Reporting summary

Further information on research design is available in the Nature Portfolio Reporting Summary linked to this article.

Data availability

Sequencing data from this study can be found on the Gene Expression Omnibus with the accession number GSE223550. Source data are provided with this paper.

Code availability

R scripts used for generating the hypoxic gene signature can be found at https://github.com/Teneth/GEND_Script.

References

42. Carraro, G. et al. Transcriptional analysis of cystic fibrosis airways at single-cell resolution reveals altered epithelial cell states and composition. *Nat. Med.* **27**, 806–814 (2021).
43. Chen, G. et al. Comprehensive identification and characterization of human secretome based on integrative proteomic and transcriptomic data. *Front. Cell Dev. Biol.* **7**, 299 (2019).
44. Hu, H. et al. AnimalTFDB 3.0: a comprehensive resource for annotation and prediction of animal transcription factors. *Nucleic Acids Res.* **47**, D33–D38 (2019).
45. Bausch-Fluck, D. et al. The in silico human surfaceome. *Proc. Natl Acad. Sci. USA* **115**, E10988–E10997 (2018).

Acknowledgements

We acknowledge support from the National Institutes of Health grants NIDDK R21DK128730 to D.D.C. and P01GM099134 to K.P., as well as from the Broad Stem Cell Research Center (BSCRC) and California NanoSystems Institute (CNSI) Stem Cell Nano-Medicine Initiative Planning Award to K.P. and D.D.C. We also acknowledge Entelexo for providing the immortalized human mesenchymal stromal cells. Sorting experiments were performed in the UCLA Jonsson Comprehensive Cancer Center (JCCC) Flow Cytometry Shared Resource that is supported by the National Institutes of Health award P30CA016042 and by the JCCC and the David Geffen School of Medicine at UCLA. We thank the Broad Stem Cell Research Center (BSCRC) and UCLA Technology Center for Genomics and Bioinformatics (TCGB) facility for assisting with sequencing. Confocal laser scanning microscopy was performed at the CNSI Advanced Light Microscopy Shared Resource Facility at UCLA. We also thank the laboratory of A. Meyer for access to the Incucyte. Selected schematic figures were created using BioRender.com.

Author contributions

S.U., J.L., J.d.R, K.P. and D.D.C. conceived the idea and contributed to the design of experiments. S.U., J.L., D.K., S.B., B.C., S.K. and C.S. performed the experiments/simulations and contributed to data analysis. S.U., J.L., K.P. and D.D.C. drafted the paper, and all the authors provided feedback. S.U. and J.L. contributed equally and have the right to list their name first in their CVs.

Competing interests

S.U., J.L., D.K., J.d.R., K.P. and D.D.C. are inventors on a patent application assigned to the University of California. J.d.R. is an employee of Partillion Bioscience, which is commercializing nanovial technology. J.d.R., D.D.C. and the University of California have financial interests in Partillion Bioscience. The other authors declare no competing interests.

Additional information

Extended data is available for this paper at https://doi.org/10.1038/s41565-023-01560-7.

Supplementary information The online version contains supplementary material available at https://doi.org/10.1038/s41565-023-01560-7.

Correspondence and requests for materials should be addressed to Kathrin Plath or Dino Di Carlo.

Peer review information *Nature Nanotechnology* thanks Klaus Eyer, Manfred Gossen and the other, anonymous, reviewer(s) for their contribution to the peer review of this work.

https://doi.org/10.1038/s41565-023-01560-7

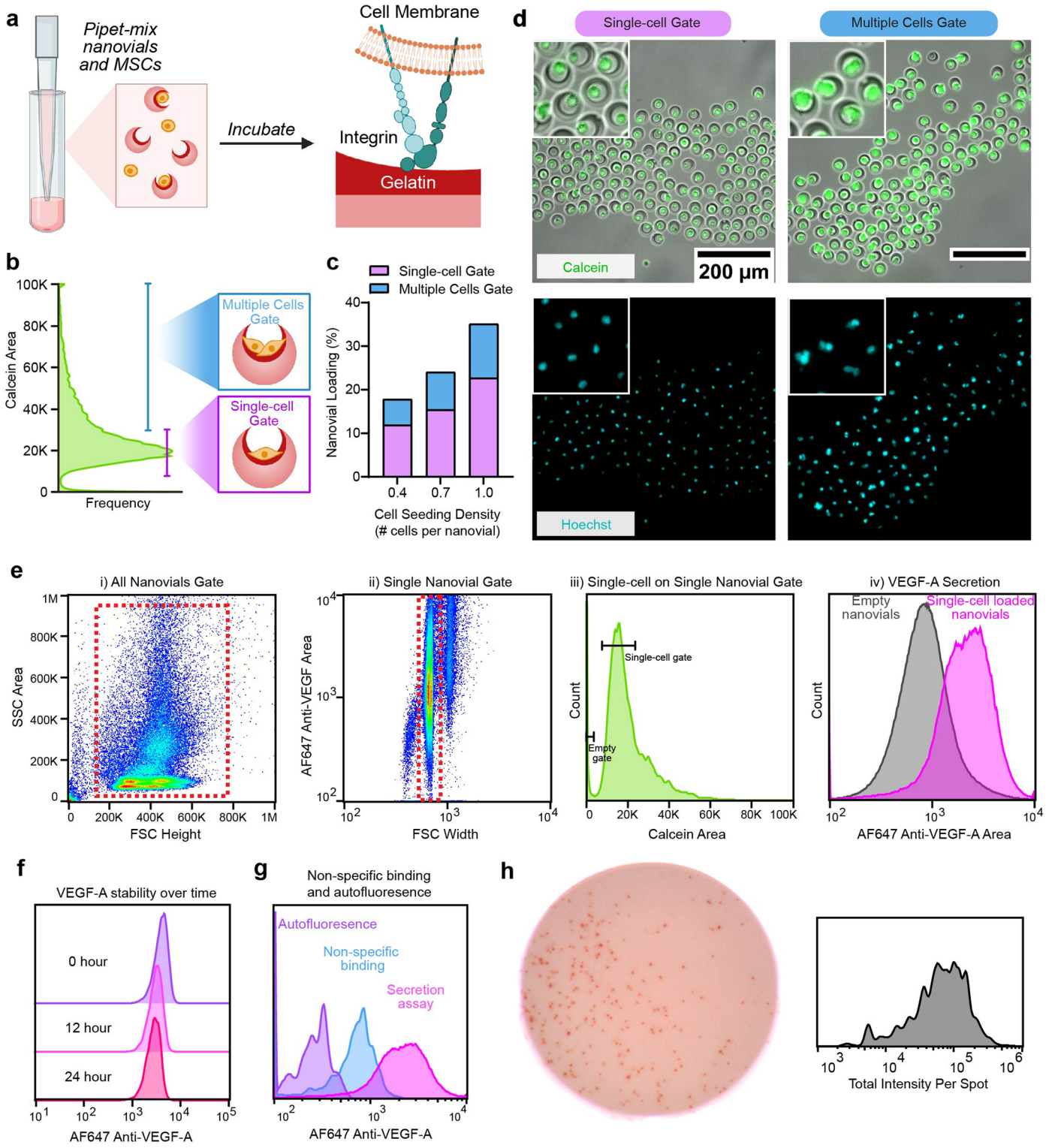

Extended Data Fig. 1 | See next page for caption.

https://doi.org/10.1038/s41565-023-01560-7

Extended Data Fig. 1 | Cell loading into nanovials, enrichment of single cell-loaded nanovials by FACS, and VEGF-A nanovial secretion assay validation. a, Anchorage of single cells on nanovials coated with gelatin via integrin binding. Cell loading into nanovials is achieved by simple mixing. **b**, Flow cytometry histogram of cell-loaded nanovials stained with calcein AM viability dye (0.4 cell per nanovial loading shown here). Cells are sorted via FACS (SONY SH800S) based on calcein signal into 'Multiple Cells' and 'Single-cell' gates. The distribution of the calcein signal has one peak with a tail at higher intensities, which represents nanovials containing more than one cell. n = 14,934 single cells events and 7,586 multiple cell events. **c**, We tested three cell loading concentrations (0.4, 0.7, and 1 cell per nanovial) and analysed the fraction of nanovials carrying zero, single or multiple cells using the gates described in (b). The graph quantifies cell loading into nanovials for these conditions. When loading cells at the 1:1 cell-to-nanovial ratio, we achieved 23% single-cell loaded nanovials which could be separated by sorting for downstream approaches and analyses. **d**, Fluorescence microscopy images of nanovials sorted for the indicated gates as described in (b). By sorting nanovials in the 'Single-cell' gate, we enriched for nanovials carrying single cells as confirmed by Hoechst nuclei staining, whereas nanovials in the tail ('Multiple Cells Gate') represented mostly two or more loaded cells. Following sorting, we estimated that 95% of the 'Single-cell' gate sorted nanovials contained one cell based on image analysis. **e**, To isolate single cells on single nanovials, the following gating strategy was used for cell-loaded nanovial samples: i) All nanovials were gated based on FSC/SSC (n = 93,263), followed by ii) a single nanovial gate based on FSC-Width (n = 80,253), and iii) the 'Single-cell' gate based on calcein signal intensity (n = 9,527). iv) Flow cytometry fluorescence histogram of the fluorescent (AF647) anti-VEGF-A detection signal in single cell-loaded nanovials and empty nanovials isolated from the same nanovial cell-loading experiment after 12 hours of secretion incubation. Single cell-loaded nanovials have higher fluorescent (AF647) anti-VEGF-A signal than empty nanovials, showing low crosstalk. **f**, Stability of recombinant VEGF-A on nanovials over 24 hours. There is a 23% decrease in AF647 Anti-VEGF-A signal from 0 to 12 hours, and a 10% decrease in signal from 12 to 24 hours. **g**, Level of autofluorescence and VEGF-A detection antibody signal for cell-loaded nanovials without VEGF-A capture/detection antibodies and cell-loaded nanovials without the VEGF-A capture antibodies, respectively. **h**, Image of one well in the ELISpot assay measuring VEGF-A secretion from MSCs. An average of 99% of cells seeded formed spots across 3 wells. The range of integrated intensity of the spots across 3 wells, quantified in the histogram on the right, indicates that there is heterogeneity in secretion level. Schematics in (a) and (b) created with BioRender.com.

https://doi.org/10.1038/s41565-023-01560-7

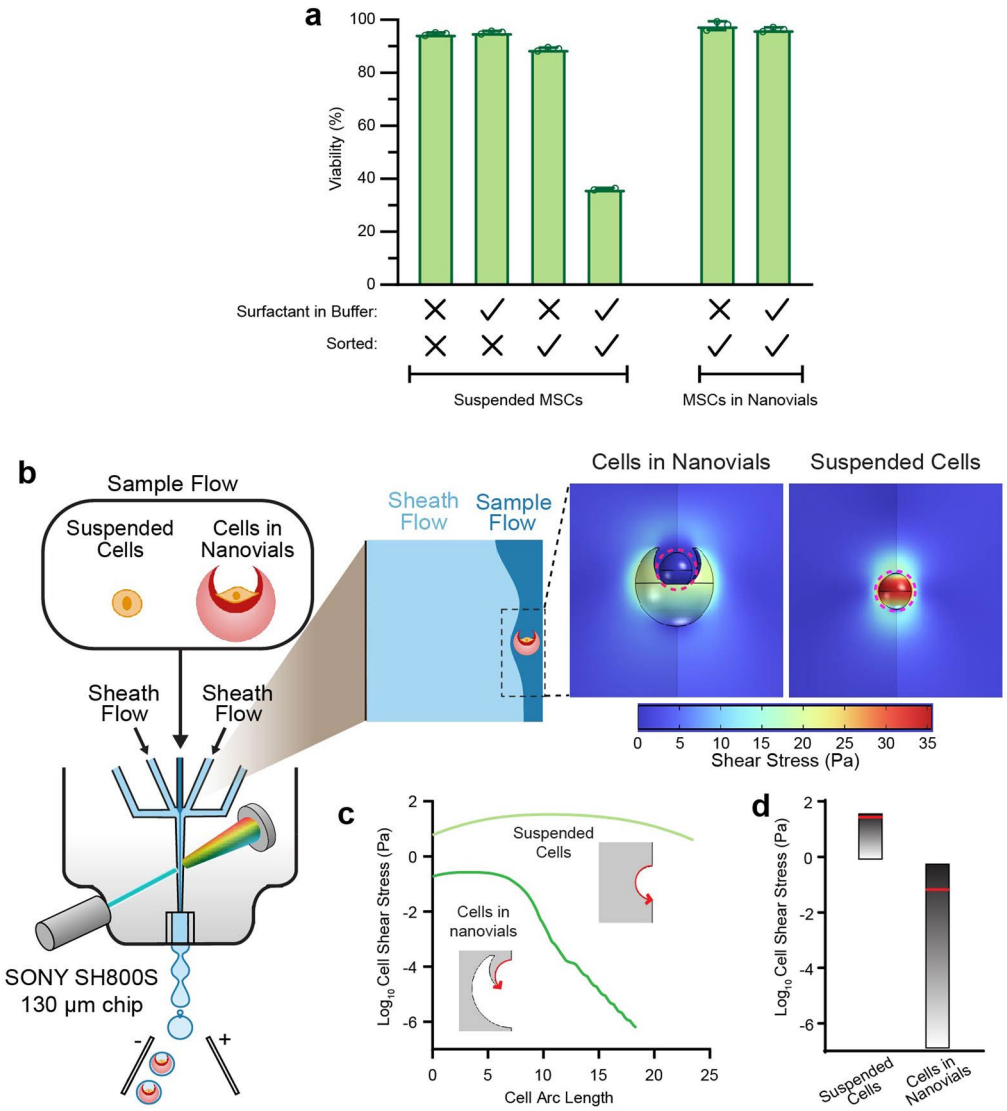

Extended Data Fig. 2 | Nanovials protect viability of MSCs during flow sorting. a, The effect of surfactant and sorting on viability of MSCs in nanovials or suspended, as measured by live/dead stain imaging. Typically, nanovial samples are kept in buffer with a surfactant (Pluronic) at low concentration for handling and sorting steps, as it prevents nanovials from aggregating. Here, we exploit the surfactant as a stressor to test the effect of sorting on the viability of suspendered cells and cells in nanovials. For suspended samples, MSCs were dissociated from flasks, resuspended in FACS buffer with and without Pluronic surfactant, and viability was measured for MSCs with and without sorting. For MSC-loaded nanovial samples, MSCs were loaded on nanovials, resuspended in wash buffer with and without Pluronic surfactant, and viability was measured for MSCs after sorting. We found that viability decreased significantly when MSCs suspended in FACS buffer with Pluronic are sorted, but all other conditions maintained high viability. Surfactant, even at low concentrations, can likely induce some membrane damage, which is enhanced during sorting; however, nanovials seem to protect cells from this damage. Data presented as mean values +/- SD for 3 replicates. **b**, Finite element modelling using COMSOL results show that cells in nanovials are exposed to reduced levels of shear stress compared to cells in suspension when flowing through the nozzle of a flow sorter (see Methods). Here, the shear stress is plotted on the cell and nozzle geometry, and shows how the suspended cell (right) experiences greater shear stress than the cell inside nanovial (left). Schematic partially created with BioRender.com. **c**, Shear stress from the COMSOL model is plotted against position along the cell perimeter for suspended cells and cells adhered within a nanovial. The red arrow in each schematic (based on the model geometry) indicates the direction of arc length and shear stress measurement. **d**, Range of shear stress for suspended cells and cells adhered within a nanovial based on (c), with average shear stress plotted (red line). The average shear stress is 400-fold higher for suspended cells than cells in nanovials.

https://doi.org/10.1038/s41565-023-01560-7

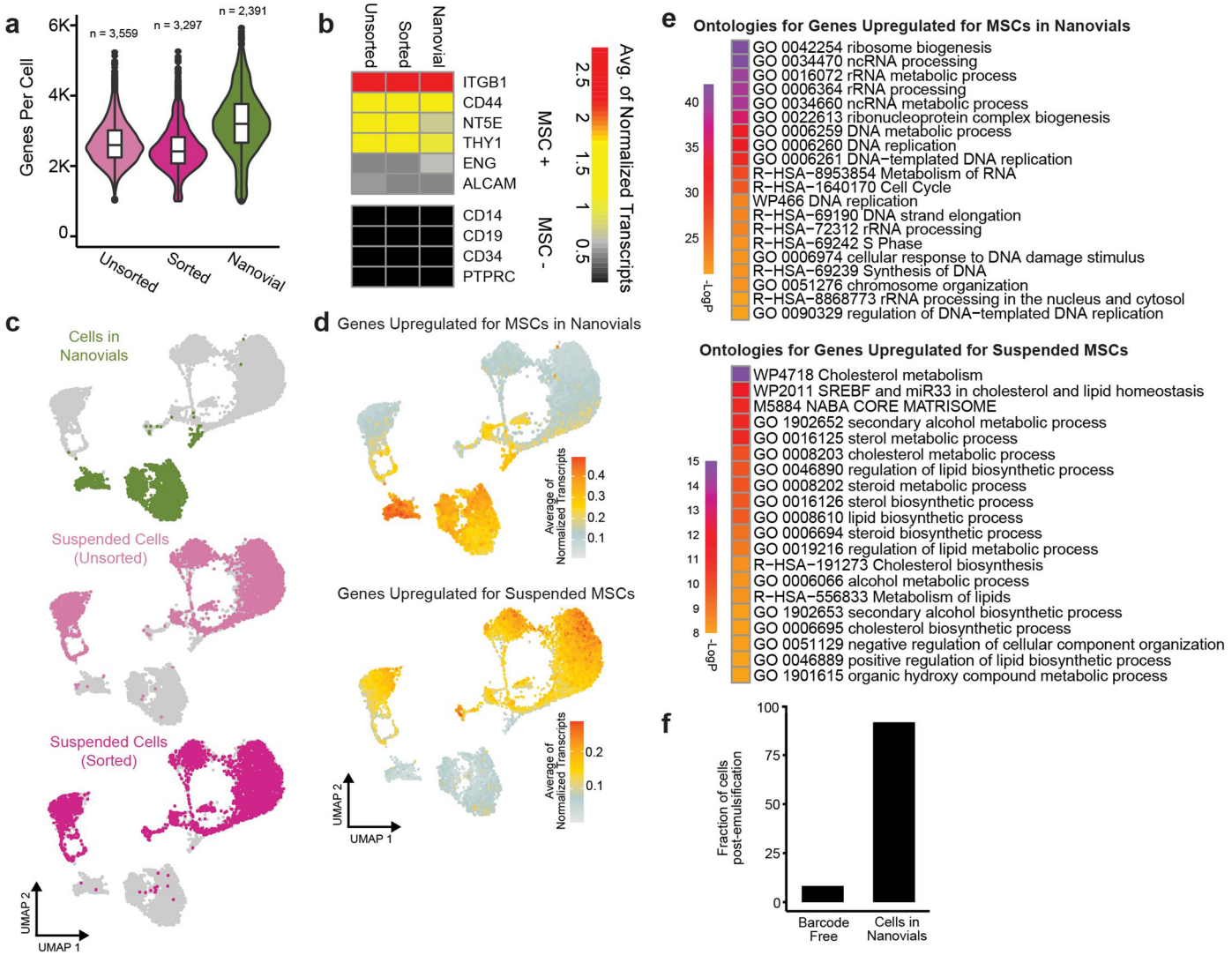

Extended Data Fig. 3 | Transcript changes related to cell loading and adhesion in nanovials. a, For the scRNA-seq experiment with MSCs loaded into nanovials or freely suspended shown in Fig. 2i, the graph shows the genes detected per cell for suspended and unsorted MSCs (unsorted), suspended FACS-sorted MSCs (sorted), and MSCs loaded on nanovials and sorted (Nanovial). **b**, Heatmap showing the average normalized transcript levels of known MSC markers (top) and markers from other cell types (bottom) in each condition from the experiment in (a). **c**, UMAPs of the combined transcriptome data from the scRNA-seq experiment described in (a). The cells from each condition are separately displayed and coloured. **d**, As in (c), showing the mean transcript level of genes significantly upregulated in cells adhered to nanovials relative to suspended MSCs (top) or upregulated in suspended MSCs (bottom). **e**, Gene ontology for the two gene sets from (d). **f**, Percent of cells with a nanovial associated oligo-barcode and the number of cells lacking such a barcode. Presumably, the cells with a barcode were still associated with a nanovial at the time of emulsification.

https://doi.org/10.1038/s41565-023-01560-7

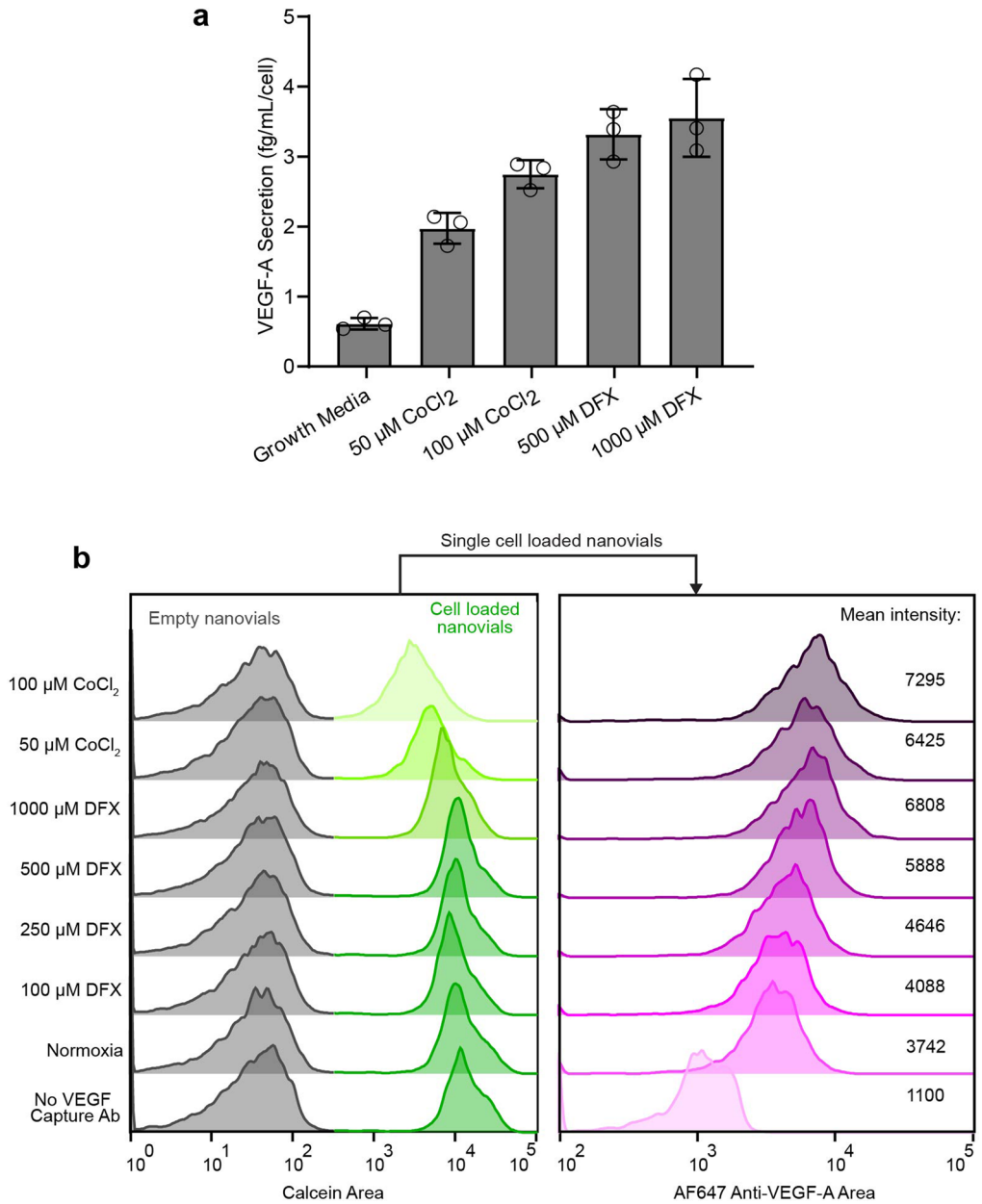

Extended Data Fig. 4 | Effect of hypoxia inducers on VEGF-A secretion by MSCs. a, ELISA for VEGF-A levels in conditioned media collected from MSCs grown on tissue culture plates under normoxic condition (normal growth media) or treated with indicated concentrations of cobalt chloride ($CoCl_2$) and deferoxamine (DFX) hypoxia mimicking agents for 24 hours to induce hypoxic conditions, as indicated. Error bars are for standard deviation. Data presented as mean values +/- SD for 3 replicates. **b**, Flow cytometry histograms for two fluorescence channels indicating calcein positive MSC-loaded nanovials with anti-VEGF-A labelling on nanovials for MSCs treated with indicated concentrations of cobalt chloride ($CoCl_2$) and deferoxamine (DFX) hypoxia mimicking agents for 14 hours total. Normoxia and control without VEGF-A capture antibody are also shown. 500 µM DFX yielded the largest increase in VEGF-A secretion (fluorescent (AF647) anti-VEGF signal) without compromising cell metabolic activity/viability (calcein).

https://doi.org/10.1038/s41565-023-01560-7

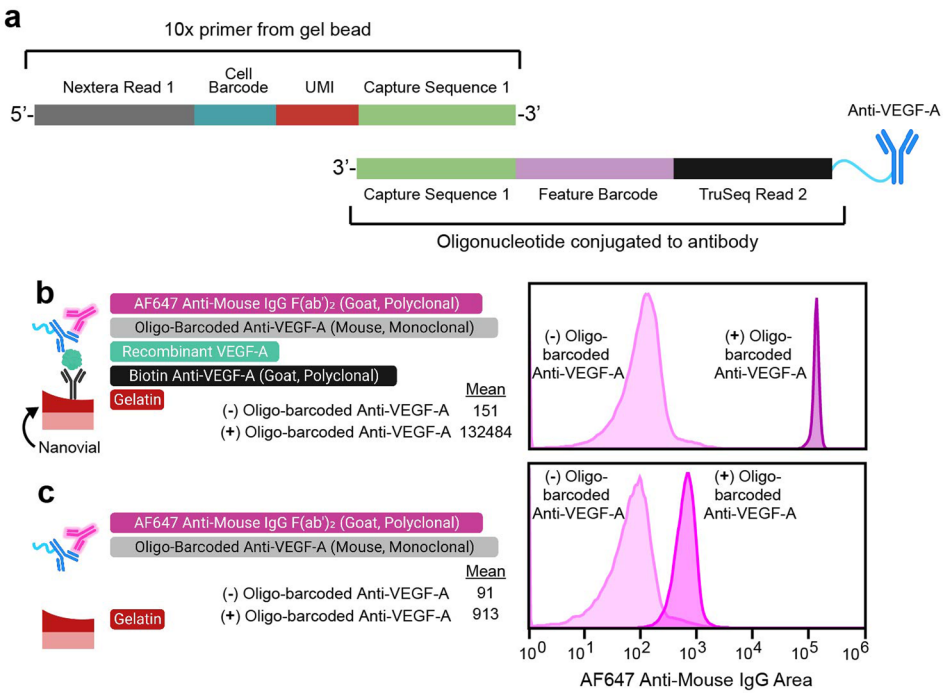

Extended Data Fig. 5 | Oligo-barcoded Anti-VEGF-A binding specificity on nanovials. a, An anti-VEGF-A antibody (used as detection antibody for VEGF-A secretion in our SEC-seq approach) was conjugated with a 10x Chromium compatible oligo-barcode along with additional sequences necessary for library preparation. The schematic shows the sequence composition of the oligo attached to the VEGF-A detection antibody, along with the 10x Chromium primer sequence which hybridizes to the antibody-derived oligo and adds the unique molecular identifier (UMI) upon reverse transcription. **b**, (Left) Schematic showing the attachment of recombinant VEGF-A and the detection immunoassay via the oligo-barcoded antibody described in (a) which was quantified with a fluorescently-labelled secondary antibody in nanovials by flow cytometry. (Right) Flow cytometry histograms showing outcome of the experiment on the left with recombinant VEGF-A with and without the oligo-barcoded VEGF-A detection antibody, demonstrating antibody specificity of the detection assay and the validity of the oligo-barcoded VEGF-A detection antibody to the presence of VEGF-A protein. The numbers on the left indicate the mean of both histograms. **c**, As in (b), except that no biotinylated anti-VEGF-A capture antibody and recombinant VEGF-A was used in the assay. Schematics in created with BioRender.com.

https://doi.org/10.1038/s41565-023-01560-7

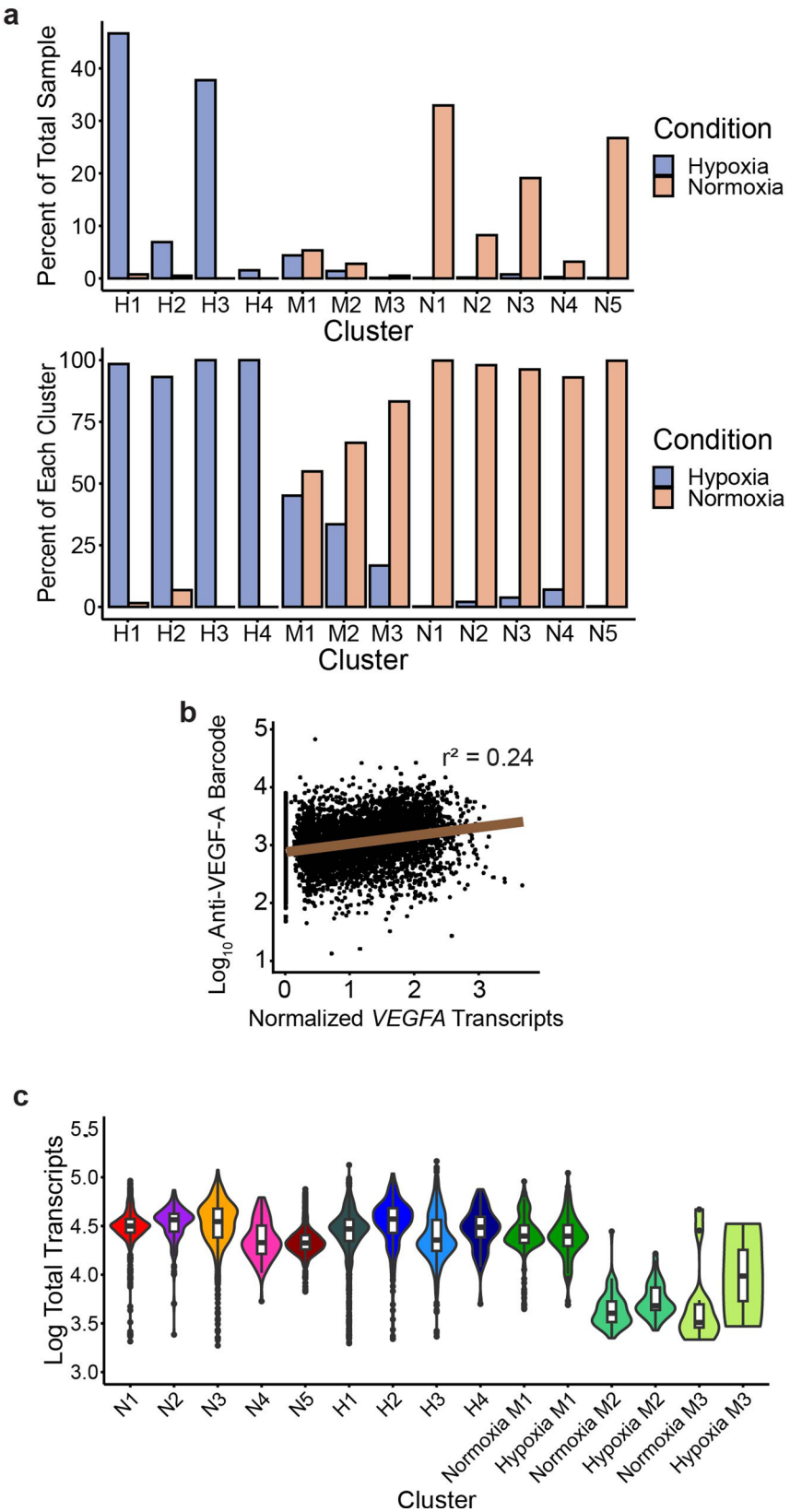

Extended Data Fig. 6 | Analysis of the SEC-seq experiments for normoxic and hypoxic MSCs. a, Proportion per cluster of hypoxic and normoxic MSCs from the SEC-seq experiments described in Fig. 3, as percent of each sample (top) or as a percent of each cluster (bottom). **b**, Scatter plot showing the correlation between *VEGFA* transcript and VEGF-A secretion for individual cells comprising hypoxic and normoxic conditions, from Fig. 3. **c**, Violin plot showing the log10 total transcript count per cell, for each cluster in Fig. 3. An overlaid box plot shows the median and first and third quartiles, in addition to the lower and upper bounds of the data. Outliers are labelled as dots.

https://doi.org/10.1038/s41565-023-01560-7

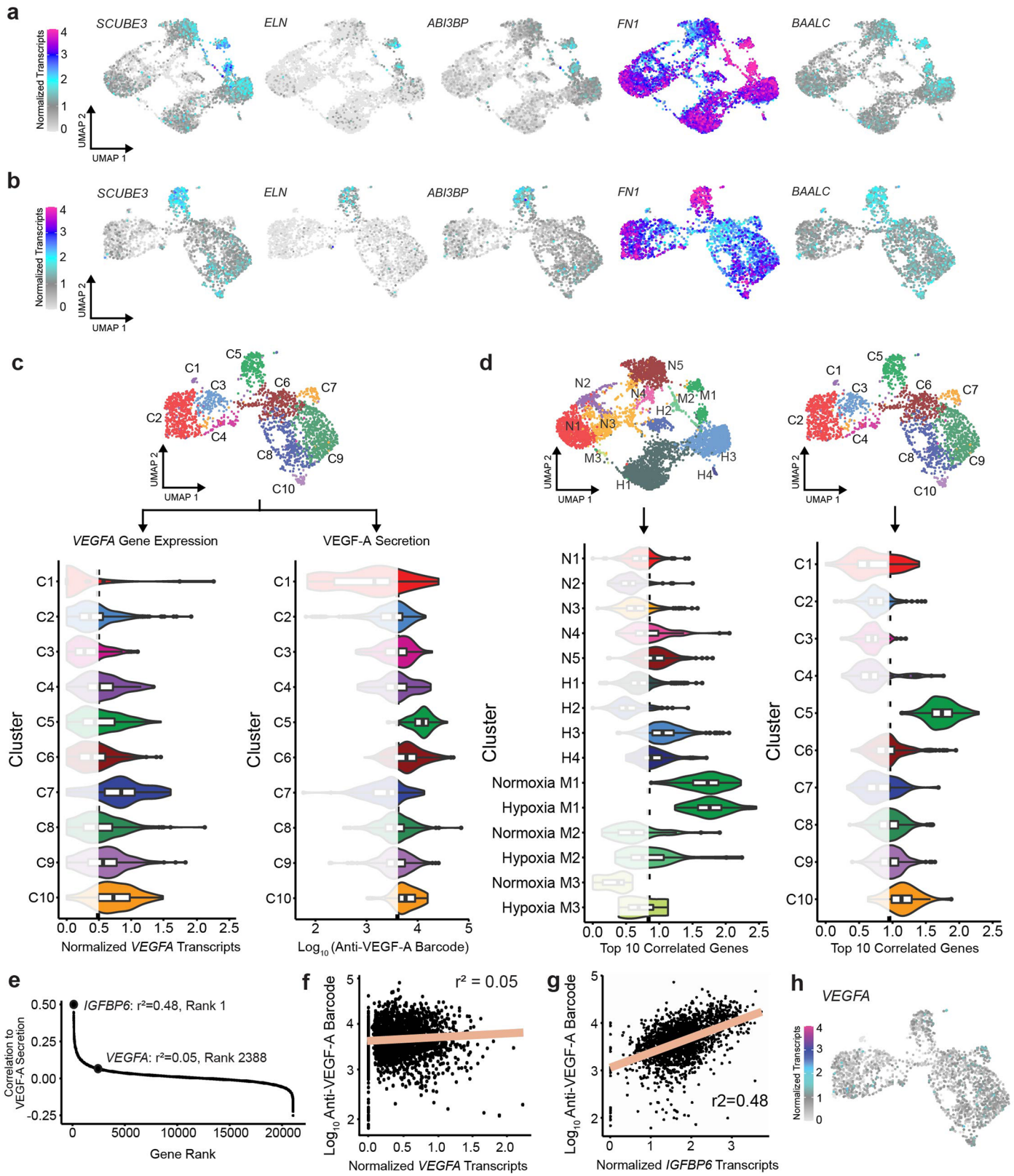

Extended Data Fig. 7 | See next page for caption.

https://doi.org/10.1038/s41565-023-01560-7

Extended Data Fig. 7 | Identification of a high-VEGF-A secreting MSC subpopulation in a replicate experiment. a, UMAPs showing the normalized transcript level of the indicated genes for the combined normoxic/hypoxic MSC SEC-seq experiments from Fig. 3. The five genes shown belong to the top 10 transcripts correlating highest with VEGF-A secretion. **b**, As in (a), for the replicate normoxic MSC SEC-seq experiment from Fig. 4d,e. **c**, UMAP with cluster information (also shown in Fig. 4e) and violin plots showing VEGF-A secretion and *VEGFA* transcript levels for all cells in each cluster in the SEC-seq experiment for normoxic MSCs from (b). Box plot shows median, 2nd and 3rd quartile, and outlier range whiskers. **d**, Violin plots showing the average normalized transcript level of the 10 highest correlating genes with VEGF-A secretion from Fig. 4b for the SEC-seq experiments with normoxic and hypoxic MSCs from Fig. 3 and the normoxic replicate from Fig. 4d,e. The UMAPs with cluster information are repeated here from the main figures for ease of interpretation. Box plot shows median, 2nd and 3rd quartile, and outlier range whiskers. **e**, For the SEC-seq experiment with normoxic MSCs in (b), all detected genes were ranked by the correlation of their transcript levels to the VEGF-A secretion level. Each gene is plotted by its rank and correlation. The ranks of the *VEGFA* and *IGFBP6* genes are highlighted and the correlation values are given. **f-g**, Scatter plots showing **f**, the correlation between *VEGFA* transcript and VEGF-A secretion for individual cells and **g**, the expression of *IGFBP6* normalized transcripts versus the log transformed VEGF-A secretion values in the replicate normoxic MSC experiment (from Fig. 4d,e). The correlation value and linear regression line are shown in each graph. **h**, UMAP showing *VEGFA* transcript levels per cell for the replicate normoxic MSC SEC-seq experiment (from Fig. 4d,e).

https://doi.org/10.1038/s41565-023-01560-7

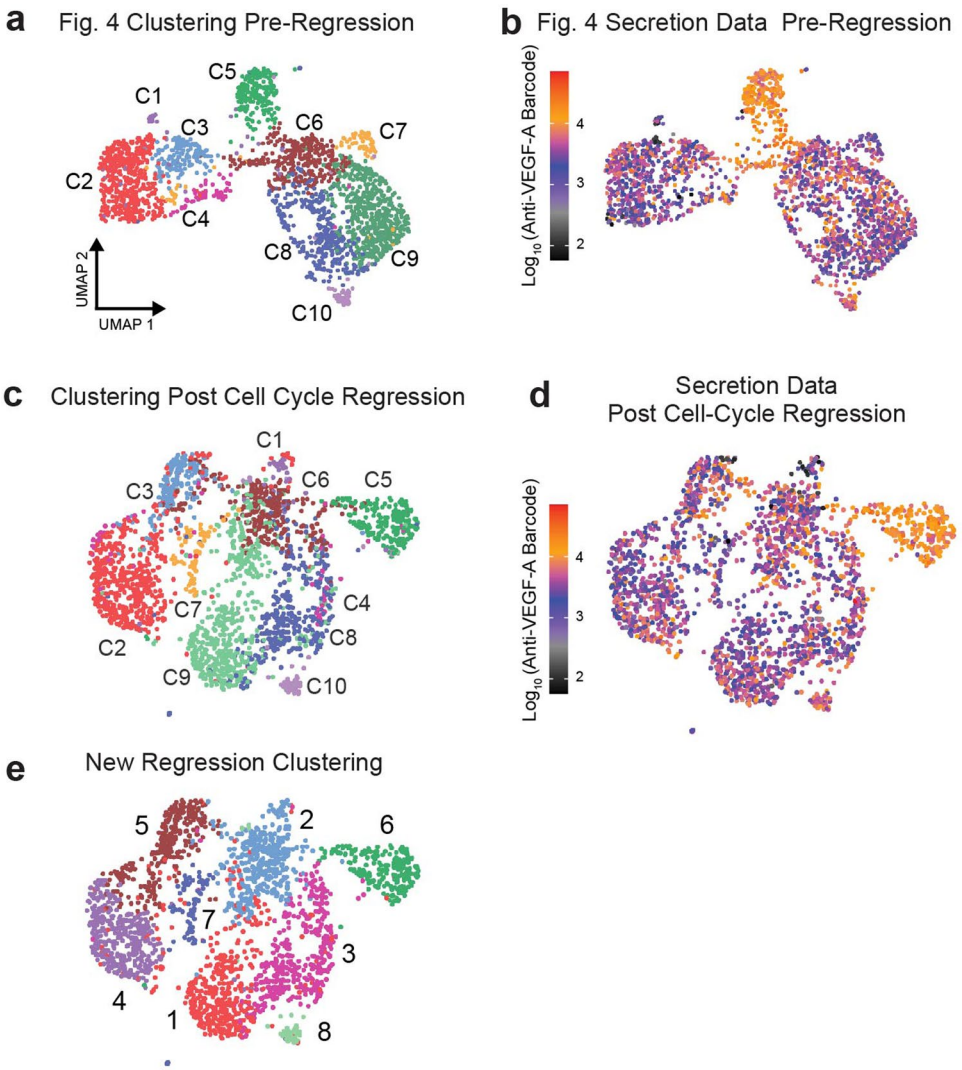

Extended Data Fig. 8 | The high VEGF-A secretion cluster is not affected by cell cycle regression. a, UMAP showing the clusters in the normoxic MSC SEC-seq replicate experiment (replicated from Fig. 4e) for easy comparison with the cell cycle-regressed data below. **b**, VEGF-A secretion per cell for the normoxic MSC SEC-seq replicate experiment (replicated from Fig. 4d) is shown for comparison with the cell cycle-regressed data below. **c**, New UMAP coordinates and clustering of normoxic cells from (a) post cell cycle regression, with the original cluster information marked. Note that Cluster C5's spatial separation from other clusters is preserved with low mixing. **d**, VEGF-A secretion shown on the new UMAP coordinates post cell cycle regression. The cells in the newly arranged cluster C5 remain highly enriched for high VEGF-A secretion. **e**, New clustering of cells post cell cycle regression displayed on the UMAP from (c). While the borders between other clusters has shifted, the majority of cells that made up cluster C5 still distinctly form their own cluster (new cluster #6), demonstrating that the highly secretion cluster's special transcriptional profile is unaffected by cell cycle information.

https://doi.org/10.1038/s41565-023-01560-7

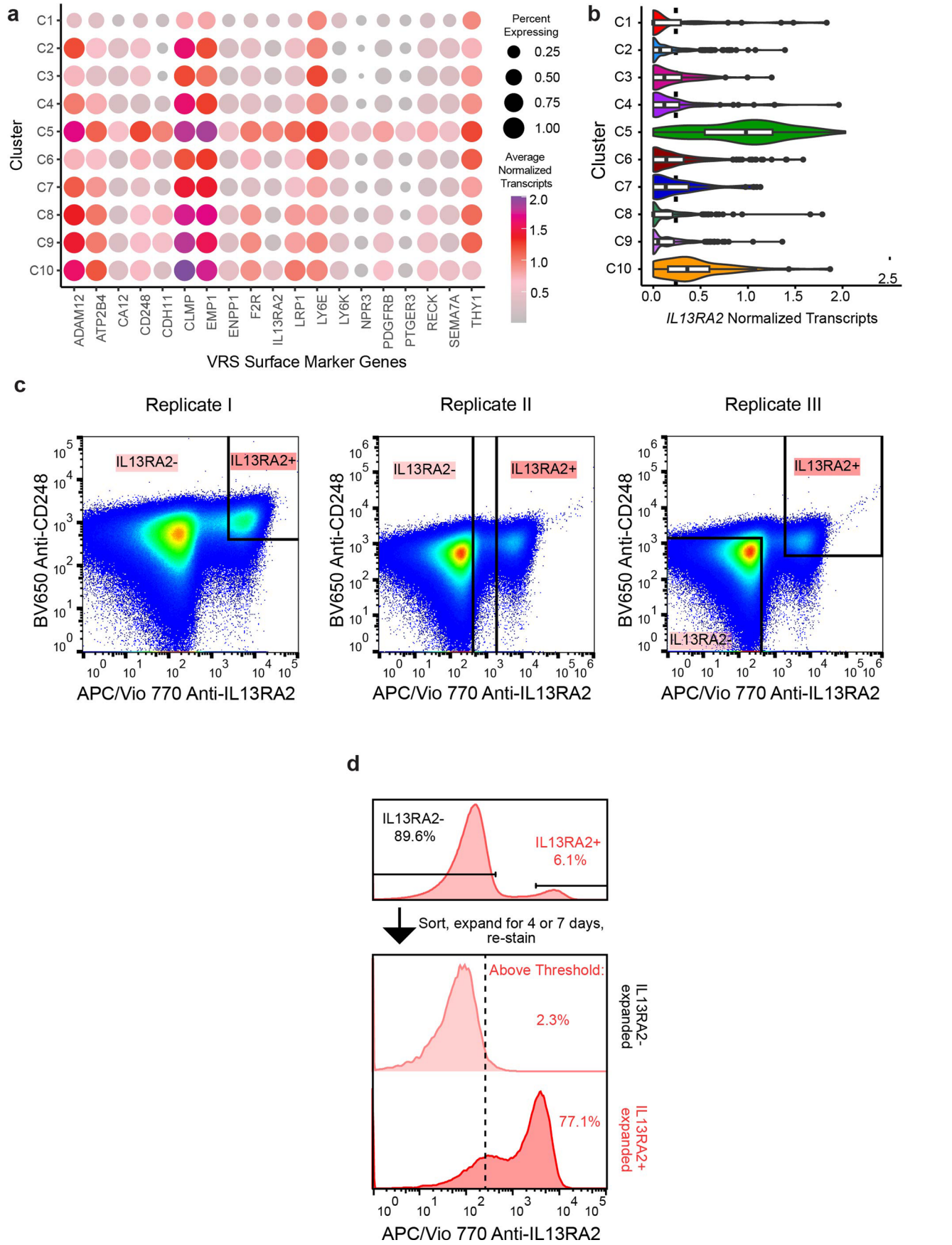

Extended Data Fig. 9 | See next page for caption.

https://doi.org/10.1038/s41565-023-01560-7

Extended Data Fig. 9 | Purification and characterization of the IL13RA2+ MSC population. a, Dot plot showing the percent of cells expressing the indicating surface marker gene as well as average normalized transcripts, for each cluster from the SEC-seq experiment in Fig. 4d,e. All surface markers shown are contained in the VRS gene list. **b**, Violin showing the normalized transcripts of *IL13RA2* for cells per cluster as labelled in Fig. 4e. The dashed line represents the mean across all cells for each plot. Box plot shows median, 2nd and 3rd quartile, and outlier range whiskers. **c**, FACS gating used for the isolation of IL13RA2+/- MSCs from three replicate experiments for downstream bulk RNA-seq. **d**, Normoxic MSCs were sorted for IL13RA2+/- subpopulations as indicated in the FACS histogram on the top. Sorted cells were expanded for 4 (IL13RA2-) or 7 (IL13RA2+) days, to account for growth differences, and subsequently stained for IL13RA2 again and analysed by flow cytometry (bottom).

https://doi.org/10.1038/s41565-023-01560-7

a

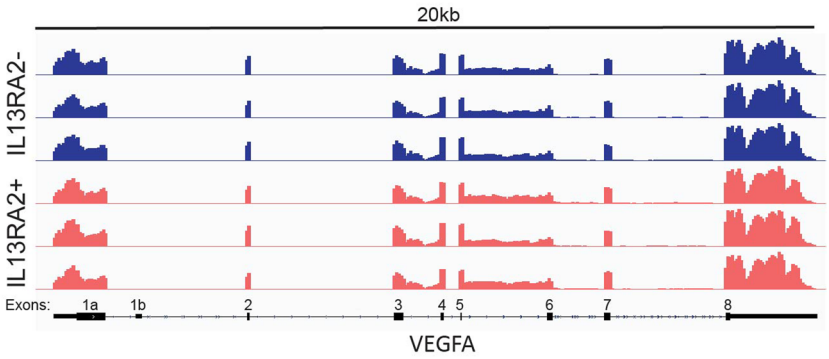

b

VEGFA Exon	Exon Start	Exon End	p-Value	FDR	Inclusion Level IL13RA2-	Inclusion Level IL13RA2+	Inclusion Diff
2	43774340	43774392	1	1	0.999	1	-0.001
4	43778459	43778536	1	1	0.999	1	-0.001
6 (1)	43780731	43780785	0.045981	0.386095	0.252	0.327	-0.075
6 (2)	43780731	43780785	0.020096	0.225231	0.076	0.113	-0.037
6 (3)	43780731	43780803	0.129877	0.674902	0.543	0.605	-0.062
6 (4)	43780731	43780803	0.039515	0.351911	0.102	0.14	-0.038
6 (5)	43780731	43780854	0.025615	0.270197	0.178	0.247	-0.069
7 (1)	43781955	43782052	0.87033	1	0.17	0.166	0.004
7 (2)	43781955	43782087	0.925025	1	0.475	0.478	-0.003
7 (3)	43781955	43782087	1	1	1	0.998	0.002
7 (4)	43781955	43782087	0.711177	1	0.977	0.98	-0.003

c

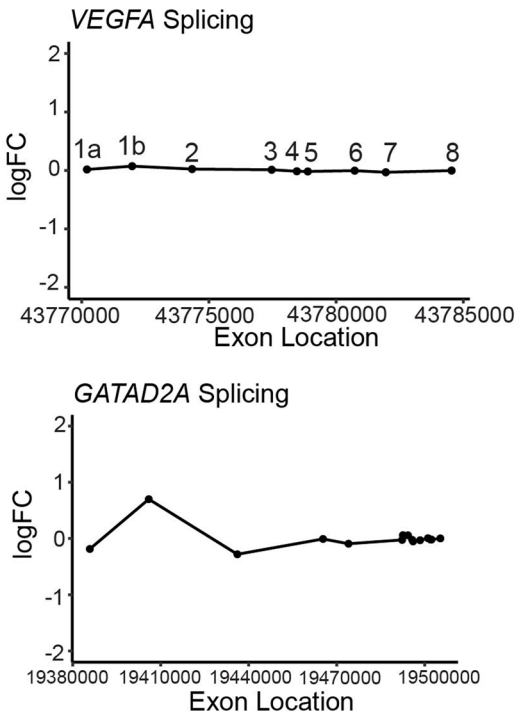

Extended Data Fig. 10 | See next page for caption.

https://doi.org/10.1038/s41565-023-01560-7

Extended Data Fig. 10 | *VEGFA* splicing from bulk RNAseq of IL13RA2+/− sorted cells. a, Integrated Genome Viewer capture of the RNA-seq reads across the *VEGFA* transcript from the triplicate bulk-RNA-seq experiments of IL13RA2-positive (red) and -negative (blue) cell populations described in Extended Data Fig. 9c. The exons of the *VEGFA* transcript are annotated below **b**, Alternative splicing output from computational evaluation of IL13RA2+ vs IL13RA2- RNA-seq libraries, grading the splicing exclusion events using only reads that span exon-exon junctions for maximum accuracy. The same exon is shown multiple times if its size varied, or it had different donor/acceptor exon pairs. Given is exon location, exclusion p-value, exclusion false discovery rate, inclusion rates and inclusion difference between samples. No exons are significantly alternatively spliced (significance threshold is $p<0.05$ & $FDR<0.10$). **c**, Top: Differential exon expression plot comparing the expression difference in *VEGFA* exon levels between the three IL13RA2+ and the three IL13RA2- samples, displayed as the log10 fold change (logFC) between the samples, where positive values indicate higher inclusion in IL13RA2+ samples. The exons are labelled. Bottom: As on the top, except for *GATAD2A* as an example of a gene with significant alternative splicing. Dots indicate the exons of this transcript.

nature portfolio

Corresponding author(s): Dino Di Carlo, Kathrin Plath

Last updated by author(s): Oct 27, 2023

Reporting Summary

Nature Portfolio wishes to improve the reproducibility of the work that we publish. This form provides structure for consistency and transparency in reporting. For further information on Nature Portfolio policies, see our Editorial Policies and the Editorial Policy Checklist.

Statistics

For all statistical analyses, confirm that the following items are present in the figure legend, table legend, main text, or Methods section.

n/a	Confirmed
☐	☒ The exact sample size (*n*) for each experimental group/condition, given as a discrete number and unit of measurement
☐	☒ A statement on whether measurements were taken from distinct samples or whether the same sample was measured repeatedly
☐	☒ The statistical test(s) used AND whether they are one- or two-sided *Only common tests should be described solely by name; describe more complex techniques in the Methods section.*
☐	☒ A description of all covariates tested
☐	☒ A description of any assumptions or corrections, such as tests of normality and adjustment for multiple comparisons
☐	☒ A full description of the statistical parameters including central tendency (e.g. means) or other basic estimates (e.g. regression coefficient) AND variation (e.g. standard deviation) or associated estimates of uncertainty (e.g. confidence intervals)
☐	☒ For null hypothesis testing, the test statistic (e.g. *F*, *t*, *r*) with confidence intervals, effect sizes, degrees of freedom and *P* value noted *Give P values as exact values whenever suitable.*
☒	☐ For Bayesian analysis, information on the choice of priors and Markov chain Monte Carlo settings
☒	☐ For hierarchical and complex designs, identification of the appropriate level for tests and full reporting of outcomes
☐	☒ Estimates of effect sizes (e.g. Cohen's *d*, Pearson's *r*), indicating how they were calculated

Our web collection on statistics for biologists contains articles on many of the points above.

Software and code

Policy information about availability of computer code

Data collection	Illumina Basespace was used to process and demultiplex raw sequencing data. 10x Genomics CellRanger was used to filter and align sequencing data.
Data analysis	R software and Seurat packages were used to analyze the sequencing data. Correlation code can be found on GitHub. Flow cytometry data was analyzed using FlowJo. Images of 10x droplets containing nanovials were analyzed with MATLAB code.

For manuscripts utilizing custom algorithms or software that are central to the research but not yet described in published literature, software must be made available to editors and reviewers. We strongly encourage code deposition in a community repository (e.g. GitHub). See the Nature Portfolio guidelines for submitting code & software for further information.

Data

Policy information about availability of data

All manuscripts must include a data availability statement. This statement should provide the following information, where applicable:

- Accession codes, unique identifiers, or web links for publicly available datasets
- A description of any restrictions on data availability
- For clinical datasets or third party data, please ensure that the statement adheres to our policy

Sequencing data from this study can be found on the Gene Expression Omnibus at accession number GSE223550. R scripts used for generating the Hypoxic gene signature can be found at https://github.com/Teneth/GEND_Script. We have provided a source date file.

Human research participants

Policy information about studies involving human research participants and Sex and Gender in Research.

Reporting on sex and gender	*Use the terms sex (biological attribute) and gender (shaped by social and cultural circumstances) carefully in order to avoid confusing both terms. Indicate if findings apply to only one sex or gender; describe whether sex and gender were considered in study design whether sex and/or gender was determined based on self-reporting or assigned and methods used. Provide in the source data disaggregated sex and gender data where this information has been collected, and consent has been obtained for sharing of individual-level data; provide overall numbers in this Reporting Summary. Please state if this information has not been collected. Report sex- and gender-based analyses where performed, justify reasons for lack of sex- and gender-based analysis.*
Population characteristics	*Describe the covariate-relevant population characteristics of the human research participants (e.g. age, genotypic information, past and current diagnosis and treatment categories). If you filled out the behavioural & social sciences study design questions and have nothing to add here, write "See above."*
Recruitment	*Describe how participants were recruited. Outline any potential self-selection bias or other biases that may be present and how these are likely to impact results.*
Ethics oversight	*Identify the organization(s) that approved the study protocol.*

Note that full information on the approval of the study protocol must also be provided in the manuscript.

Field-specific reporting

Please select the one below that is the best fit for your research. If you are not sure, read the appropriate sections before making your selection.

☒ Life sciences ☐ Behavioural & social sciences ☐ Ecological, evolutionary & environmental sciences

For a reference copy of the document with all sections, see nature.com/documents/nr-reporting-summary-flat.pdf

Life sciences study design

All studies must disclose on these points even when the disclosure is negative.

Sample size	We had three SEC-seq samples, each with at least 2000 cells each.
Data exclusions	Typical filtering was performed to exclude cells with low quality or mixed identity.
Replication	The normoxic treated mesenchymal stromal cells SEC-seq experiment was replicated and the results were recapitulated.
Randomization	Single-cell sequencing randomly samples thousands of cells to eliminate bias.
Blinding	The entire sample was used for SEC-seq, therefore we were blinded to subpopulation bias.

Reporting for specific materials, systems and methods

We require information from authors about some types of materials, experimental systems and methods used in many studies. Here, indicate whether each material, system or method listed is relevant to your study. If you are not sure if a list item applies to your research, read the appropriate section before selecting a response.

Materials & experimental systems

n/a	Involved in the study
☐	☒ Antibodies
☐	☒ Eukaryotic cell lines
☒	☐ Palaeontology and archaeology
☒	☐ Animals and other organisms
☒	☐ Clinical data
☒	☐ Dual use research of concern

Methods

n/a	Involved in the study
☒	☐ ChIP-seq
☐	☒ Flow cytometry
☒	☐ MRI-based neuroimaging

Antibodies

Antibodies used	Biotin anti-human VEGF Antibody, clone: Poly5225 (Biolegend, 522503) Anti-VEGF Antibody, Alexa Fluor® 647 Conjugate (Sigma-Aldrich, ABS82-AF647) TotalSeq-B 5136 anti-human VEGF Antibody, clone: A15136H (Biolegend, custom antibody conjugation) Alexa Fluor 647 AffiniPure F(ab')$_2$ Fragment Goat Anti-Mouse IgG, F(ab')$_2$ fragment specific (Jackson Immunoresearch, 115-606-072) CD213α2 (IL-13Rα2) Antibody, anti-human, APC-Vio 770, REAfinity (Miltenyi, 130-104-506) BD OptiBuild BV650 Mouse Anti-Human Endosialin (CD248) (Becton Dickinson, 743902)
Validation	Biotin anti-human VEGF Antibody was validated by ELISA by manufacturer. Anti-VEGF Antibody, Alexa Fluor® 647 Conjugate was validated by immunocytochemistry analysis to detect VEGF in HeLa cells by manufacturer. We also validated the specificity by testing it on nanovials with and without recombinant human VEGF-A and measuring resulting signal by flow cytometry. TotalSeq-B 5136 anti-human VEGF Antibody was validated by us by testing it on nanovials with and without recombinant human VEGF-A and measuring resulting signal by flow cytometry using a secondary antibody. Alexa Fluor 647 AffiniPure F(ab')$_2$ Fragment Goat Anti-Mouse IgG was validated by manufacturer to react with the F(ab')$_2$ portion of mouse IgG by immunoelectrophoresis and/or ELISA. It was also tested by the manufacturer by ELISA and/or solid-phase adsorbed to ensure minimal cross-reaction with human, bovine, and horse serum proteins.

Eukaryotic cell lines

Policy information about cell lines and Sex and Gender in Research

Cell line source(s)	Immortalized adipose-derived mesenchymal stem cells are from ATCC (SCRC-4000). They are from the adipose tissue of a White female.
Authentication	By manufacturer.
Mycoplasma contamination	Immortalized adipose-derived mesenchymal stem cells tested negative for mycoplasma contamination.
Commonly misidentified lines (See ICLAC register)	n/a

Flow Cytometry

Plots

Confirm that:

☒ The axis labels state the marker and fluorochrome used (e.g. CD4-FITC).

☒ The axis scales are clearly visible. Include numbers along axes only for bottom left plot of group (a 'group' is an analysis of identical markers).

☒ All plots are contour plots with outliers or pseudocolor plots.

☒ A numerical value for number of cells or percentage (with statistics) is provided.

Methodology

Sample preparation	Nanovials were loaded with cells. After straining, nanovials were incubated for 12 hours to allow for secretion or directly used for non-secretion experiments. Then nanovial samples were stained with necessary antibodies and cell stains. Finally, nanovial samples were resuspended in wash buffer (0.05% Pluronic F-127, 0.5% Bovine Serum Albumin, 1% antibiotic-antimycotic in PBS).
Instrument	SONY SH800S Cell Sorter
Software	SH800S software was used to collect the flow cytometry data. FlowJo (BD) was used to analyze the flow cytometry data.
Cell population abundance	Typically 10-20% of nanovials had single cells loaded, as detected by calcein signal intensity. Purity was determined by image analysis.
Gating strategy	'All nanovials' were first gated from all events using a threshold of 120,000 FSC-Height and 40,000 SSC-Area. Next, 'single nanovials' were gated from 'All nanovials' between 600 and 900 FSC-Width. Lastly, 'single cells on single nanovials' were gated from 'single nanovials' by creating a gate centered around the calcein positive peak, which is thresholded at a minimum of 3000.

☒ Tick this box to confirm that a figure exemplifying the gating strategy is provided in the Supplementary Information.